

GeV - PeV Neutrino Production and Oscillation in hidden jets from GRBs

Nissim Fraija ^{*}

*Instituto de Astronomía, Universidad Nacional Autónoma de México, Circuito Exterior,
C.U., A. Postal 70-264, 04510 México D.F., México*

19 October 2021

ABSTRACT

Long gamma-ray bursts have been widely associated with collapsing massive stars in the framework of collapsar model. High-energy neutrinos and photons can be produced in the internal shocks of middle relativistic jets from core-collapse supernova. Although photons can hardly escape, high-energy neutrinos could be the only signature when the jets are hidden. We show that using suitable parameters, high-energy neutrinos in GeV - PeV range can be produced in the hidden jet inside the collapsar, thus demonstrating that these objects are candidates to produce neutrinos with energies between 1 - 10 PeV which were observed with IceCube. On the other hand, due to matter effects, high-energy neutrinos may oscillate resonantly from one flavor to another before leaving the star. Using two (solar, atmospheric and accelerator parameters) and three neutrino mixing, we study the possibility of resonant oscillation for these neutrinos created in internal shocks. Also we compute the probabilities of neutrino oscillations in the matter at different distances along the jet (before leaving the star) and after in vacuum, on their path to Earth. Finally, neutrino flavor ratios on Earth are estimated.

Key words: Long Gamma-ray burst: High-energy Neutrinos: – Neutrino Oscillation

1 INTRODUCTION

A number of different high-energy, ≥ 1 GeV, neutrino sources have been proposed in literature, that include active galactic nuclei (AGNs) (Stecker et al. 1991; Szabo & Protheroe 1994; Nellen, Mannheim & Biermann 1993; Atoyan & Dermer 2001; Alvarez-Muñiz & Mészáros 2004), gamma-ray bursts (GRBs) (Waxman & Bahcall 1997; Dermer & Atoyan 2003; Razzaque, Mészáros & Waxman 2004; Murase et al. 2006; Gupta & Zhang 2007), supernova remnants (Alvarez-Muñiz & Halzen 2002; Costantini & Vissani 2005) and core collapse supernovae (Waxman & Loeb 2001; Wang et al. 2007), although long duration GRBs have been found to be tightly connected with core-collapse supernovae (Hjorth & et al. 2003; Stanek & et al. 2003). Properties of neutrino fluxes, energy range, shape of the energy spectra and flavor content depend on physical conditions in the sources. Neutrinos are useful for studying sources, especially when photons cannot escape directly. They could be the only prompt signatures of the “hidden” sources. These have been associated to core collapse of massive stars leading to supernovae (SNe) of type Ib,c and II with mildly relativistic jets emitted by a central engine, a black hole or a highly magnetized neutron star. Depending on the initial density and metallicity, the pre-supernova star could have different radii. Type Ic supernovae are believed to be He stars with radius $R_* \approx 10^{11}$ cm and

Supernovae of type II and Ib are thought to have a radius of $R_* \approx 3 \times 10^{12}$ cm.

Recently, IceCube reported the detection of two neutrino-induced events with energies between 1- 10 PeV (IceCube Collaboration et al. 2013a). These events have been discussed as having an extragalactic origin, for instance; GRBs (Cholis & Hooper 2012) and low-luminosity GRBs (Liu & Wang 2013). On the other hand, high-energy neutrinos are produced in the decay of charged pions and muons when energetic protons in the jet interact with synchrotron thermalized photons or nucleons/mesons (pp, pn)/(π , K) in the shocks. For internal shocks, synchrotron radiation and the number density of particles could be calculated with enough accuracy if we know the distribution of the magnetic field and the particle momentum in the shocked region. These quantities are calculated using the energy equipartition hypothesis through the equipartition parameters; electron equipartition ($\epsilon_e = U_e/U$) and magnetic equipartition $\epsilon_B = U_B/U$ (Meszaros, Rees & Wijers 1998). Many authors (Barniol Duran, Bošnjak & Kumar 2012; Fraija, González & Lee 2012; Sacahui et al. 2012; Kumar & Barniol Duran 2010; Shen, Kumar & Piran 2010) have estimated these parameters to be $\epsilon_e \simeq 0.1$, and $0.1 \leq \epsilon_B \leq 10^{-4}$, to obtain a good description of more than a dozen of GRBs.

On the other hand, the neutrino flavor ratio is expected to be, at the source, $\phi_{\nu_e}^0 : \phi_{\nu_\mu}^0 : \phi_{\nu_\tau}^0 = 1 : 2 : 0$ and on Earth (due to neutrino oscillations between the source and Earth) $\phi_{\nu_e}^0 : \phi_{\nu_\mu}^0 : \phi_{\nu_\tau}^0 = 1 : 1 :$

^{*} E-mail: nifraija@astro.unam.mx. Luc Binette-Fundación UNAM Fellow.

1 and $\phi_{\nu_e}^0 : \phi_{\nu_\mu}^0 : \phi_{\nu_\tau}^0 = 1 : 1.8 : 1.8$ for neutrino energies less and greater than 100 TeV, respectively, for gamma ray bursts ($\phi_{\nu_i}^0$ is the sum of ν_i and $\bar{\nu}_i$) (Kashti & Waxman 2005). Also it has been pointed out that measurements of the deviation of this standard flavor ratio of astrophysical high-energy neutrinos may probe new physics (Learned & Pakvasa 1995; Athar, Jeżabek & Yasuda 2000; Kashti & Waxman 2005). As it is known, neutrino properties get modified when it propagates in a medium. Depending on their flavor, neutrinos interact via neutral and/or charged currents, for instance, ν_e interacts with electrons via both neutral and charged currents, whereas ν_ν (ν_τ) interacts only via the neutral current. This induces a coherent effect in which maximal conversion of ν_e into ν_μ (ν_τ) takes place. The resonant conversion of neutrino from one flavor to another due to the medium effect is well known as the Mikheyev-Smirnov-Wolfenstein effect (Wolfenstein 1978). Resonance condition of high-energy neutrinos in hidden jets has been studied in the literature (Mena, Mocioiu & Razzaque 2007; Razzaque & Smirnov 2010; Sahu & Zhang 2010). Recently, Osorio Oliveros, Sahu & Sanabria (2013) studied the three-flavor neutrino oscillations on the surface of the star for neutrino energy in the range (0.1 - 100) TeV. They found that those neutrinos generated on the surface with energies of less than 10 TeV could oscillate. Unlike previous studies, we show that these sources are capable of generating PeV neutrinos pointing them out as possible progenitors of the first observation of PeV-energy neutrinos with IceCube (IceCube Collaboration et al. 2013a). Besides, we do a full analysis of resonance conditions (two- and three-flavors) for neutrinos produced at different places in the star, estimating the flavor ratios on Earth.

In this paper we both show that PeV neutrinos can be produced in hidden jets and estimate the flavor ratio of high-energy neutrinos expected on Earth. Firstly, we compute the energy range of neutrinos produced by cooling down of hadrons and mesons accelerated in a mildly relativistic jet. After that we take different matter density profiles to show that neutrinos may oscillate resonantly depending on the neutrino energy and mixing neutrino parameters. Finally, we discuss our results in the fail jet framework.

2 JET DYNAMICS

For the internal shocks, we consider a mildly relativistic shock propagating with bulk Lorentz factor $\Gamma_b = 10^{0.5} \Gamma_{b,0.5}$. Behind the shock, the comoving number density of particles and density of energy are $n'_e = n'_p = 1/(8\pi m_p c^5) \Gamma_b^{-4} E_j t_{\nu,s}^{-2} t_j^{-1} = 3.1 \times 10^{18} \text{ cm}^{-3} t_{\nu,s}^{-2}$ and $n'_p m_p c^2$, respectively, where we have taken the set of typical values for which the jet drills but hardly breaks through the stellar envelope: the jet kinetic energy $E_j = 10^{51.5} E_{j,51.5}$ erg, the variability time scale of the central object $t_\nu = t_{\nu,s}$ s with $t_{\nu,s} = 0.1$ and 0.01 , and the jet duration $t_j = 10 t_{j,1}$ s (Razzaque, Mészáros & Waxman 2005; Ando & Beacom 2005; MacLachlan et al. 2013). We assume that electrons and protons are accelerated in the internal shocks to a power-law distribution $N(\gamma_j) d\gamma_j \propto \gamma_j^{-p} d\gamma_j$. The internal shocks due to shell collisions take place at a radius $r_j = 2\Gamma_b^2 c t_\nu = 6 \times 10^{11} \text{ cm} \Gamma_{b,0.5}^2 t_{\nu,s}$. Electrons, with minimum energy $E_{e,m} = \frac{p-2}{p-1} \epsilon_e m_p c^2 \Gamma_b$ and maximum energy limited by the dynamic time scale $t'_{dyn} \simeq t_\nu \Gamma_b$, cool down rapidly by synchrotron radiation in the presence of the magnetic field given by

$$B' = \left(\frac{\epsilon_B}{c^3} \Gamma_b^{-4} E_j t_{\nu}^{-2} t_j^{-1} \right)^{1/2}$$

$$= 3.43 \times 10^8 \text{ G} \Gamma_{b,0.5}^{-2} E_{j,51.5}^{1/2} t_{j,1}^{-1/2} \epsilon_B^{1/2} t_{\nu,s}^{-1}, \quad (1)$$

where here and further on the magnetic equipartition parameter and $t_{\nu,s}$ lie in the range $0.1 \leq \epsilon_B \leq 10^{-4}$ and $0.1 \leq t_{\nu,s} \leq 0.01$, respectively. The radiated photon energies by electron synchrotron emission with energy E_e is $E_{syn,\gamma} = eB'/(hm_e^3 c^5) E_e^2$, and also the opacity to Thomson scattering by these photons is

$$\begin{aligned} \tau'_{th} &= \frac{\sigma_T}{4\pi m_p c^4} \Gamma_b^{-3} E_j t_{\nu}^{-1} t_j^{-1} \\ &= 3.9 \times 10^5 \Gamma_{b,0.5}^{-3} E_{j,51.5} t_{j,1}^{-1} t_{\nu,s}^{-1}. \end{aligned} \quad (2)$$

Due to the large Thomson optical depth, synchrotron photons will thermalize to a black body temperature, therefore the peak energy is given by

$$\begin{aligned} E'_\gamma \sim k_B T_\gamma &= \left(\frac{15(\hbar c)^3}{8\pi^4 c^3} \right)^{1/4} \epsilon_e^{1/4} E_j^{1/4} \Gamma_b^{-1} t_{\nu}^{-1/2} t_j^{-1/4} \\ &= 1.36 \text{ keV} E_{j,51.5}^{1/4} \Gamma_{b,0.5}^{-1} t_{j,1}^{-1/4} \epsilon_{e,-1}^{1/4} t_{\nu,s}^{-1/2}, \end{aligned} \quad (3)$$

and the number density of thermalized photons is

$$\begin{aligned} n'_\gamma &= \frac{2\zeta(3)}{\pi^2 (c\hbar)^3} \left(\frac{15\hbar\epsilon_e E_j}{8\pi^4 \Gamma_b^4 t_{\nu}^2 t_j} \right)^{3/4} \\ &= 2.86 \times 10^{23} \text{ cm}^{-3} E_{j,51.5}^{3/4} \Gamma_{b,0.5}^{-3} t_{j,1}^{-3/4} \epsilon_{e,-1}^{3/4} t_{\nu,s}^{-3/2}. \end{aligned} \quad (4)$$

Although keV photons can hardly escape due to the high optical depth, they are able to interact with relativistic protons accelerated in the jet, producing high-energy neutrinos via charged pion decay. The pion energies depend on the proton energy and characteristics of the jet.

3 HADRONIC MODEL

Protons accelerated in internal shocks, on the one hand, radiate photons by synchrotron radiation and also scatter the internal photons by inverse Compton (IC) scattering, and on the other hand, interact with thermal keV photons and hadrons by $p\gamma$ and p -hadron interactions. The optical depths for $p\gamma$ and p -hadron interactions are

$$\begin{aligned} \tau'_{p\gamma} &= \frac{4\zeta(3)\sigma_{p\gamma}}{\pi^2 (c\hbar)^3} \left(\frac{15\hbar\epsilon_e E_j}{8\pi^4 \Gamma_b^{8/3} t_{\nu}^{2/3} t_j} \right)^{3/4} \\ &= 3.19 \times 10^6 E_{j,51.5}^{3/4} \Gamma_{b,0.5}^{-2} t_{j,-1}^{-3/4} \epsilon_{e,-1}^{3/4} t_{\nu,s}^{-1/2}, \end{aligned} \quad (5)$$

and

$$\begin{aligned} \tau'_{pp} &= \frac{\sigma_{pp}}{4\pi m_p c^5} E_j \Gamma_b^{-3} t_{\nu}^{-1} t_j^{-1} \\ &= 1.77 \times 10^4 E_{j,51.5} \Gamma_{b,0.5}^{-3} t_{j,1}^{-1} t_{\nu,s}^{-1}, \end{aligned} \quad (6)$$

respectively. Due to the optical depths for $p\gamma$ and p -hadron interactions are very high, $p\gamma$ and p -hadron are effective, although p -hadron interactions are more effective at lower energy than $p\gamma$ interactions (Razzaque, Mészáros & Waxman 2004).

3.1 Cooling time scales

The shock acceleration time for an energy proton, E'_p , is

$$\begin{aligned} t'_{acc} &= \frac{2\pi\xi}{c} r_L = \frac{2\pi\xi c^{1/2} B'_{c,p}}{m_p^2} E'_p \epsilon_B^{-1/2} E_j^{-1/2} \Gamma_b^2 t_\nu t_j^{1/2} \\ &= 2.04 \times 10^{-12} \text{ s} E'_p \xi E_{j,51.5}^{-1/2} \Gamma_{b,0.5}^2 t_{j,1}^{1/2} \epsilon_B^{-1/2} t_{\nu,s}, \end{aligned} \quad (7)$$

where r_L is the Larmor's radius and ξ is a factor of equality. The acceleration time, t'_{acc} , gives an account of the maximum proton

energy achieved, when it is compared with the maximum cooling time scales. In the following subsections we are going to calculate the cooling time scales for protons and mesons.

3.1.1 Proton cooling time scales

The cooling time scale for proton synchrotron radiation is

$$\begin{aligned} t'_{p, syn} &= \frac{E'_p}{(dE'_p/dt)_{syn}} = \frac{6\pi m_p^4 c^6}{\sigma_T \beta^2 m_e^2 E'_p} \epsilon_B^{-1} E_j^{-1} \Gamma_b^4 t_v^2 t_j \\ &= 38.3 \text{ s } E_{p,9}'^{-1} E_{j,51.5}'^{-1} \Gamma_{b,0.5}^4 t_{j,1} \epsilon_B^{-1} t_{\nu,s}^2. \end{aligned} \quad (8)$$

Protons in the shock region can upscatter the thermal keV photons $E'_{IC,\gamma} \sim \gamma_p^2 E'_\gamma$ with peak energy and density given in eqs.(3) and (4). The IC cooling time scale in the Thomson regimen is

$$\begin{aligned} t'_{p,ic} &= \frac{E'_p}{(dE'_p/dt)_{ic}^{th}} = \frac{m_p^4 c^4 \pi^6 (c\hbar)^2}{5\sigma_T \beta^2 m_e^2 \zeta(3) E'_p} \epsilon_e^{-1} E_j^{-1} \Gamma_b^4 t_v^2 t_j \\ &= 383.1 \text{ s } E_{p,9}'^{-1} E_{j,51.5}'^{-1} \Gamma_{b,0.5}^4 t_{j,1} \epsilon_{e,-1}^{-1} t_{\nu,s}^2. \end{aligned} \quad (9)$$

Also, the IC cooling time scale in the Klein-Nishina (KN) regimen, $E'_p E'_\gamma / m_p^2 c^4 = \Gamma_{KN}$ with $(\Gamma_{KN} = 1)$, is

$$\begin{aligned} t'_{p,ic}^{KN} &= \frac{E'_p}{(dE'_p/dt)_{ic}^{KN}} = \frac{3\pi^4 (c\hbar)^3 E'_p \epsilon_e^{-1/2} E_j^{-1/2} \Gamma_b^2 t_v t_j^{1/2}}{2\sqrt{30}\hbar \sigma_T \beta^2 m_e^2 c^5 \zeta(3)} \\ &= 5.15 \times 10^{-10} \text{ s } E_{p,9}'^{-1/2} E_{j,51.5}'^{-1/2} \Gamma_{b,0.5}^2 t_{j,1}^{1/2} \epsilon_{e,-1}^{-1/2} t_{\nu,s}. \end{aligned} \quad (10)$$

On the other hand, protons could upscatter thermal photons according to Bethe-Heitler (BH) process. The proton energy loss is taken away by the pairs produced in this process. The cooling time scale for the BH scattering is

$$\begin{aligned} t'_{BH} &= \frac{E'_p}{(dE'_p/dt)_{BH}} = \frac{E'_p}{n' c \sigma_{BH} \Delta E'_p} \\ &= \frac{E'_p (m_p^2 c^4 + 2E'_p E'_\gamma)^{1/2}}{2n'_\gamma m_e c^3 \sigma_{BH} (E'_p + E'_\gamma)}, \end{aligned} \quad (11)$$

where $\sigma_{BH} = \alpha r_e^2 ((28/9) \ln[2E'_p E'_\gamma / (m_p m_e c^4)] - 106/9)$. The energy loss rate due to pion production for $p\gamma$ interactions is (Stecker 1968; Becker & Biermann 2009)

$$\begin{aligned} t'_{p\gamma} &= \frac{\pi^2 (c\hbar)^3}{0.3 c \sigma_{p\gamma} \zeta(3)} \left(\frac{8\pi^4 \Gamma_b^4 t_v^2 t_j}{15 \hbar \epsilon_e E_j} \right)^{3/4} \\ &= 1.32 \times 10^{-5} \text{ s } E_{j,51.5}'^{-3/4} \Gamma_{b,0.5}^3 t_{j,1}^{3/4} \epsilon_{e,-1}^{-3/4} t_{\nu,s}^{3/2}, \end{aligned} \quad (12)$$

and for p-hadron interactions is (Dermer & Atoyan 2003; Dermer & Menon 2009)

$$\begin{aligned} t'_{pp} &= \frac{10\pi m_p c^4}{\sigma_{pp}} E_j^{-1} \Gamma_b^4 t_v^2 t_j \\ &= 4.47 \times 10^{-4} \text{ s } E_{j,51.5}'^{-1} \Gamma_{b,0.5}^4 t_{j,1} t_{\nu,s}^2. \end{aligned} \quad (13)$$

In figs 1 and 2 we have plotted the proton cooling time scales when the magnetic field is distributed in order to $0.1 \leq \epsilon_B \leq 10^{-4}$ and internal shocks take place at $r=6 \times 10^9$ cm and $r=6 \times 10^{10}$ cm, respectively.

3.1.2 Meson cooling time scales

High-energy charged pions and kaons produced by p-hadron and $p\gamma$ interactions ($p + \gamma/p \rightarrow X + \pi^\pm/K^\pm$) radiate in the presence of the magnetic field (eq. 1). Therefore, their cooling time scales are

$$t'_{\pi^\pm, syn} = \frac{E'_{\pi^\pm}}{(dE'_{\pi^\pm}/dt)} \simeq \frac{6\pi c^6 m_{\pi^\pm}^4}{\sigma_T \beta^2 m_e^2} \epsilon_B^{-1} E_j^{-1} \Gamma_b^2 t_v^2 t_j E_{\pi^\pm}'^{-1}$$

$$= 1.9 \times 10^{-2} \text{ s } E_{\pi^\pm,9}'^{-1} E_{j,51.5}'^{-1} \Gamma_{b,0.5}^2 t_{j,1} \epsilon_B^{-1} t_{\nu,s}^2 \quad (14)$$

and

$$\begin{aligned} t'_{K^\pm, syn} &= \frac{E'_{K^\pm}}{(dE'_{K^\pm}/dt)} \simeq \frac{6\pi c^6 m_{K^\pm}^4}{\sigma_T \beta^2 m_e^2} \epsilon_B^{-1} E_j^{-1} \Gamma_b^2 t_v^2 t_j E_{K^\pm}'^{-1} \\ &= 2.94 \text{ s } E_{K^\pm,9}'^{-1} E_{j,51.5}'^{-1} \Gamma_{b,0.5}^2 t_{j,1} \epsilon_B^{-1} t_{\nu,s}^2. \end{aligned} \quad (15)$$

As protons can collide with secondary pions and kaons ($\pi^+ p$ and $K^+ p$), then its respective cooling time scale is given by

$$\begin{aligned} t'_{had} &= \frac{10\pi m_p c^4}{\sigma_{(pK/p\pi^+)}} E_j^{-1} \Gamma_b^4 t_v^2 t_j \\ &= 4.47 \times 10^{-9} \text{ s } E_{j,51.5}'^{-1} \Gamma_{b,0.5}^4 t_{j,1} t_{\nu,s}^2. \end{aligned} \quad (16)$$

Here we have used the cross-section $\sigma_{(pK/p\pi^+)} \approx 3 \times 10^{-26} \text{ cm}^2$. Because the mean lifetime of these mesons may be comparable with the synchrotron and hadron time scales in some energy range, it is necessary to consider the cooling time scales related to their mean lifetime which are given by

$$\begin{aligned} t'_{\pi^\pm, dec} &= \frac{E'_{\pi^\pm}}{m_{\pi^\pm} c^2 \tau_{\pi^\pm}} \\ &= 1.87 \times 10^{-7} \text{ s } E_{\pi^\pm,9}', \end{aligned} \quad (17)$$

and

$$\begin{aligned} t'_{K^\pm, dec} &= \frac{E'_{K^\pm}}{m_{K^\pm} c^2 \tau_{K^\pm}} \\ &= 2.51 \times 10^{-8} \text{ s } E_{K^\pm,9}', \end{aligned} \quad (18)$$

where τ_{π^\pm/K^\pm} is the mean lifetime for π^\pm/K^\pm and $E_{\pi^\pm/K^\pm,9}' = 10^9 E_{\pi^\pm/K^\pm} \text{ eV}$.

In figs 3 and 4 we have plotted the meson cooling time scales when internal shocks happen at $r=6 \times 10^9$ cm and $r=6 \times 10^{10}$ cm and the magnetic equipartition parameter is in the range $0.1 \leq \epsilon_B \leq 10^{-4}$.

3.2 Neutrino production

The single-pion production channels are $p + \gamma \rightarrow n + \pi^+$ and $p + \gamma \rightarrow p + \pi^0$, where the relevant pion decay chains are $\pi^0 \rightarrow 2\gamma$, $\pi^+ \rightarrow \mu^+ + \nu_\mu \rightarrow e^+ + \nu_e + \bar{\nu}_\mu + \nu_\mu$ and $\pi^- \rightarrow \mu^- + \bar{\nu}_\mu \rightarrow e^- + \bar{\nu}_e + \nu_\mu + \bar{\nu}_\mu$ (Dermer & Atoyan 2003), then the threshold neutrino energy from $p\gamma$ interaction is

$$\begin{aligned} E'_{\nu,\pi} &= 2.5 \times 10^{-2} \left(\frac{8\pi^4}{15\hbar} \right)^{1/4} \frac{(m_\Delta^2 - m_p^2)}{(1 - \cos\theta)} \\ &\quad \times \epsilon_e^{-1/4} E_j^{-1/4} \Gamma_b t_v^{1/2} t_j^{1/4} \\ &= 9.72 \text{ TeV } E_{j,51.5}'^{-1/4} \Gamma_{b,0.5} t_{j,1}^{1/4} \epsilon_{e,-1}^{-1/4} t_{\nu,s}^{1/2}. \end{aligned} \quad (19)$$

Comparing the time cooling scales we can estimate the neutrino break energy for each process. Equating $t_{acc} \simeq t'_{p, syn}$, we can approximately estimate the maximum proton energy

$$\begin{aligned} E'_{p, max} &= \left(\frac{3e m_p^4 c^{11/2}}{\sigma_T \xi \beta^2 m_e^2} \right)^{1/2} \epsilon_B^{-1/4} E_j^{-1/4} \Gamma_b t_v^{1/2} t_j^{1/4} \\ &= 4.3 \times 10^3 \text{ GeV } E_{j,51.5}'^{-1/4} \Gamma_{b,0.5} t_{j,1}^{1/4} \epsilon_B^{-1/4} t_{\nu,s}^{1/2}. \end{aligned} \quad (20)$$

From the condition of the synchrotron cooling time scales for mesons ($t'_{\pi^\pm, syn} = t'_{had}$ and $t'_{K^\pm, syn} = t'_{had}$), one may roughly define the neutrino break energies as

$$\begin{aligned} E'_{\nu,\pi^\pm, syn} &= 0.15 \times \frac{m_{\pi^\pm}^4 c^2 \sigma_{pp}}{m_p \sigma_T \beta^2 m_e^2} \epsilon_B^{-1} \\ &= 10.5 \text{ GeV } \epsilon_B^{-1}, \end{aligned} \quad (21)$$

and

$$\begin{aligned} E'_{\nu, k^+ syn} &= 0.3 \times \frac{m_{k^+}^4 c^2 \sigma_{pp}}{m_p \sigma_T \beta^2 m_e^2} \epsilon_B^{-1} \\ &= 3.28 \text{ TeV } \epsilon_B^{-1}. \end{aligned} \quad (22)$$

From the lifetime condition of cooling time scale ($t'_{\pi^+, dec} = t'_{had}$ and $t'_{K^+, dec} = t'_{had}$), one again we can obtain the neutrino break energies, which for these cases are

$$\begin{aligned} E'_{\nu, \pi^+ lt} &= 2.5 \frac{\pi m_p m_{\pi^+} c^6}{\sigma_{pp}} \tau_{\pi^+}^{-1} E_j^{-1} \Gamma_b^4 t_v^2 t_j \\ &= 0.6 \text{ TeV } E_{j, 51.5}^{-1} \Gamma_{b, 0.5}^4 t_{j, 1} t_{\nu, s}^2, \end{aligned} \quad (23)$$

and

$$\begin{aligned} E'_{\nu, k^+ lt} &= 5 \frac{\pi m_p m_{k^+} c^6}{\sigma_{pp}} \tau_{k^+}^{-1} E_j^{-1} \Gamma_b^4 t_v^2 t_j \\ &= 8.92 \text{ TeV } E_{j, 51.5}^{-1} \Gamma_{b, 0.5}^4 t_{j, 1} t_{\nu, s}^2. \end{aligned} \quad (24)$$

It is important to say that muons may be suppressed by electromagnetic energy losses and in that case would not contribute much to high-energy neutrino production. The ratio $\frac{t'_{\pi^+/K^+, cool}}{t'_{\pi^+/K^+, dec}}$,

where $t'_{\pi^+/K^+, cool} = \frac{t'_{\pi^+/K^+, em} \cdot t'_{\pi^+/K^+, had}}{t'_{\pi^+/K^+, em} + t'_{\pi^+/K^+, had}}$, determines the suppression of mesons before they decay to neutrinos (Razzaque, Mészáros & Waxman 2005).

In fig. 5 we have plotted the neutrino energy created by distinct interaction processes at different distances, 6×10^9 cm (above) and 6×10^{10} cm (below), as a function of the magnetic equipartition parameter.

4 DENSITY PROFILE OF THE SOURCE

Analytical and numerical models of density distribution in a pre-supernova have shown a decreasing dependence on radius $\rho \propto r^{-n}$, with $n=3/2 - 3$ above the core, being $3/2$ and 3 convective and radiative envelopes respectively (Woosley, Langer & Weaver 1993; Shigeyama & Nomoto 1990; Arnett 1991). In particular, distributions with $\rho \propto r^{-3}$ and $\rho \propto r^{-17/7}$ have been proposed to describe simple blast wave distributions (Bethe & Pizzochero 1990; Chevalier & Soker 1989). Following Mena, Mocioiu & Razzaque (2007), we use three models of density profile; Model [A], Model [B] and Model [C].

Model [A],

$$[A] \quad \rho(r) = 4.0 \times 10^{-6} \left(\frac{R_*}{r} - 1 \right)^3 \text{ g cm}^{-3}, \quad (25)$$

corresponds to a polytropic hydrogen envelope with $\rho(r) \propto r^{-3}$, scaling valid in the range $r_{jet} \geq r \geq R_*$. Model [B],

$$\begin{aligned} [B] \quad \rho(r) &= 3.4 \times 10^{-5} \text{ g cm}^{-3} \\ &\times \begin{cases} (R_*/r)^{17/7}; & 10^{10.8} \text{ cm} < r < r_b = 10^{12} \text{ cm} \\ (R_*/r_b)^{17/7} (r - R_*)^5 / (r_b - R_*)^5; & r > r_b, \end{cases} \end{aligned} \quad (26)$$

is a power-law fit with an effective polytropic index $n_{eff} = 17/7$ as done for SN 1987A (Chevalier & Soker 1989). Here $r_j \sim 10^{10.8}$ cm is the radius of inner border of the envelope, where the density $\rho = 0.4 \text{ g cm}^{-3}$. Associating the number of electron per nucleon $Y_e = 0.5$, we obtained the number density of electrons as $N_e = N_a \rho(r) Y_e = 1.2 \times 10^{23} \text{ cm}^{-3}$ and Model [C],

$$[C] \quad \rho(r) = 6.3 \times 10^{-6} A \left(\frac{R_*}{r} - 1 \right)^{n_{eff}} \text{ g cm}^{-3}$$

$$(n_{eff}, A) = \begin{cases} (2.1, 20); & 10^{10.8} \text{ cm} < r < 10^{11} \text{ cm} \\ (2.5, 1); & r > 10^{11} \text{ cm}, \end{cases} \quad (27)$$

includes a sharp drop in density at the edge of the helium core (Matzner & McKee 1999).

5 NEUTRINO MIXING

In the following subsections we are going to describe the neutrino oscillations in the matter (along the jet for three density profiles given in section 4) and in vacuum (its path up to Earth). We will be using the best fit parameters for two-neutrino mixing (solar, atmospheric and accelerator neutrino experiments) and three-neutrino mixing. The best fit value of solar, atmospheric and accelerator neutrino experiments are given as follow.

Solar Neutrinos are electron neutrinos produced in the thermonuclear reactions which generate the solar energy. The Sudbury Neutrino Observatory (SNO) was designed to measure the flux of neutrinos produced by ^8B decays in the sun, so-called ^8B neutrinos, and to study neutrino oscillations, as proposed by Chen (1985). A two-flavor neutrino oscillation analysis gave the following parameters: $\delta m^2 = (5.6_{-1.4}^{+1.9}) \times 10^{-5} \text{ eV}^2$ and $\tan^2 \theta = 0.427_{-0.029}^{+0.033}$ (Aharmim & et al. 2011).

Atmospheric Neutrinos are electron neutrinos ν_e produced mainly from the decay chain $\pi \rightarrow \mu + \nu_\mu$ followed by $\mu \rightarrow e + \nu_\mu + \nu_e$. Super-Kamiokande (SK) observatory observes interactions between neutrinos with electrons or with nuclei or water via the water Cherenkov method. Under a two-flavor disappearance model with separate mixing parameters between neutrinos and antineutrinos there were found the following parameters for the SK-I + II + III data: $\delta m^2 = (2.1_{-0.4}^{+0.9}) \times 10^{-3} \text{ eV}^2$ and $\sin^2 2\theta = 1.0_{-0.07}^{+0.00}$ (Abe & et al. 2011).

Reactor Neutrinos are produced in Nuclear reactors. Kamioka Liquid scintillator Anti-Neutrino Detector (KamLAND) was initially designed to detect reactor neutrinos and so later it was prepared to measure ^7Be solar neutrinos. A two neutrino oscillation analysis gives $\delta m^2 = (7.9_{-0.5}^{+0.6}) \times 10^{-5} \text{ eV}^2$ and $\tan^2 \theta = 0.4_{-0.07}^{+0.10}$ (Araki & et al. 2005; Shirai & KamLAND Collaboration 2007; the KamLAND Collaboration & Mitsui 2011).¹

Accelerator Neutrinos are mostly produced by π decays (and some K decays), with the pions produced by the scattering of the accelerated protons on a fixed target. The beam can contain both μ - and e-neutrinos and antineutrinos. There are two categories: Long and short baselines.

Long-baseline experiments with accelerator beams run with a baseline of about a hundred of kilometers. K2K experiment was designed to measure neutrino oscillations using a man-made beam with well controlled systematics, complementing and confirming the measurement made with atmospheric neutrinos. $\delta m^2 = (2.8_{-0.9}^{+0.7}) \times 10^{-3} \text{ eV}^2$ and $\sin^2 2\theta = 1.0$ (Ahn & et al. 2006).

Short-baseline experiments with accelerator beams run with a baseline of about hundreds of meters. Liquid Scintillator Neutrino Detector (LSND) was designed to search for $\nu_\mu \rightarrow \nu_e$ oscillations using ν_μ from π^+ decay in flight (Athanasopoulos & et al. 1996, 1998). The region of parameter space has been partly tested by Karlsruhe Rutherford medium energy neutrino KAR-MEN (Armbruster & et al. 2002) and MiniBooNe experiments. Church et al. (2002) found two well-defined regions of oscillation

¹ this value was obtained using a global analysis of data from KamLAND and solar-neutrino experiments

parameters with either $\delta m^2 \approx 7 \text{ eV}^2$ or $\delta m^2 < 1 \text{ eV}^2$ compatible with both LAND and KARMEN experiments, for the complementary confidence. The MiniBooNE experiment was specially designed to verify the LSND's neutrino data. It is currently running at Fermilab and is searching for ν_e ($\bar{\nu}_e$) appearance in a ν_μ ($\bar{\nu}_\mu$) beam. Although MiniBooNE found no evidence for an excess of ν_e candidate events above 475 MeV in the $\nu_\mu \rightarrow \nu_e$ study, there was observed a 3.0σ excess of electron-like events below 475 MeV (Aguilar-Arevalo & et al. 2009, 2010, 2007). In addition, in the $\bar{\nu}_\mu \rightarrow \bar{\nu}_e$ study, MiniBooNE found evidence of oscillations in the 0.1 to 1.0 eV^2 , which are consistent with LSND results (Athanassopoulos & et al. 1996, 1998).

Combining solar, atmospheric, reactor and accelerator parameters, the best fit values of the three neutrino mixing are

for $\sin^2_{13} < 0.053$: (Aharmim & et al. 2011)

$$\Delta m^2_{21} = (7.41^{+0.21}_{-0.19}) \times 10^{-5} \text{ eV}^2; \tan^2 \theta_{12} = 0.446^{+0.030}_{-0.029}, \quad (28)$$

and for $\sin^2_{13} < 0.04$: (Wendell & et al. 2010)

$$\Delta m^2_{23} = (2.1^{+0.5}_{-0.2}) \times 10^{-3} \text{ eV}^2; \sin^2 \theta_{23} = 0.50^{+0.083}_{-0.093} \quad (29)$$

5.1 Neutrino oscillation inside the jet

When neutrino oscillations take place in the matter, a resonance could occur that dramatically enhances the flavor mixing and can lead to maximal conversion from one neutrino flavor to another. This resonance depends on the effective potential, density profile of the medium, and oscillation parameters. As ν_e is the one that can interact via CC, the effective potential can be obtained calculating the difference between the potential due to CC and NC contributions (Kuo & Pantaleone 1989).

5.1.1 Two-Neutrino Mixing

In this subsection, we will consider the neutrino oscillation process $\nu_e \leftrightarrow \nu_\mu, \nu_\tau$. The evolution equation for the propagation of neutrinos in the above medium is given by

$$i \begin{pmatrix} \dot{\nu}_e \\ \dot{\nu}_\mu \end{pmatrix} = \begin{pmatrix} V_{eff} - \Delta \cos 2\theta & \frac{\Delta}{2} \sin 2\theta \\ \frac{\Delta}{2} \sin 2\theta & 0 \end{pmatrix} \begin{pmatrix} \nu_e \\ \nu_\mu \end{pmatrix}, \quad (30)$$

where $\Delta = \delta m^2 / 2E_\nu$, $V_{eff} = \sqrt{2}G_F N_e$ is the effective potential, E_ν is the neutrino energy, and θ is the neutrino mixing angle. For anti-neutrinos one has to replace N_e by $-N_e$. The conversion probability for a given time t is

$$P_{\nu_e \rightarrow \nu_\mu(\nu_\tau)}(t) = \frac{\Delta^2 \sin^2 2\theta}{\omega^2} \sin^2 \left(\frac{\omega t}{2} \right), \quad (31)$$

with

$$\omega = \sqrt{(V_{eff} - \Delta \cos 2\theta)^2 + \Delta^2 \sin^2 2\theta}. \quad (32)$$

The oscillation length for the neutrino is given by

$$L_{osc} = \frac{L_v}{\sqrt{\cos^2 2\theta (1 - \frac{V_{eff}}{\Delta \cos 2\theta})^2 + \sin^2 2\theta}}, \quad (33)$$

where $L_v = 2\pi/\Delta$ is the vacuum oscillation length. If the density of the medium is such that the condition $\sqrt{2}G_F N_e = \Delta \cos 2\theta$ is satisfied, the resonant condition,

$$V_{eff,R} = \Delta \cos 2\theta, \quad (34)$$

can come about, therefore the resonance length can be written as

$$L_{res} = \frac{L_v}{\sin 2\theta}. \quad (35)$$

Combining eqs (35) and (34) we can obtain the resonance density as a function of resonance length

$$\rho_R = \begin{cases} \left[\frac{3.69 \times 10^{-4}}{E_{\nu, TeV}} \left[1 - E_{\nu, TeV}^2 \left(\frac{4.4 \times 10^{12} \text{ cm}}{l_r} \right)^2 \right]^{1/2} \right] \text{ gr/cm}^3 & \text{sol. ,} \\ \left[\frac{1.39 \times 10^{-2}}{E_{\nu, TeV}} \left[1 - E_{\nu, TeV}^2 \left(\frac{1.18 \times 10^{11} \text{ cm}}{l_r} \right)^2 \right]^{1/2} \right] \text{ gr/cm}^3 & \text{atmosp. ,} \\ \left[\frac{3.29}{E_{\nu, TeV}} \left[1 - E_{\nu, TeV}^2 \left(\frac{4.9 \times 10^8 \text{ cm}}{l_r} \right)^2 \right]^{1/2} \right] \text{ gr/cm}^3 & \text{accel. ,} \end{cases} \quad (36)$$

where sol, atmosp. and accel. correspond to solar, atmospheric and accelerator parameters.

In addition of the resonance condition, the dynamics of this transition must be determined by adiabatic conversion through the adiabaticity parameter

$$\gamma \equiv \frac{\delta m^2}{2E} \sin 2\theta \tan 2\theta \frac{1}{\left| \frac{1}{\rho} \frac{d\rho}{dr} \right|_R}, \quad (37)$$

with $\gamma \gg 1$ or the flip probability given by

$$P_f = e^{-\pi/2\gamma}, \quad (38)$$

where ρ is given by eqs. (25), (26) and (27).

5.1.2 Three-neutrino Mixing

To determine the neutrino oscillation probabilities we have to solve the evolution equation of the neutrino system in the matter. In a three-flavor framework, this equation is given by

$$i \frac{d\vec{\nu}}{dt} = H\vec{\nu}, \quad (39)$$

and the state vector in the flavor basis is defined as

$$\vec{\nu} \equiv (\nu_e, \nu_\mu, \nu_\tau)^T. \quad (40)$$

The effective Hamiltonian is

$$H = U \cdot H_0^d \cdot U^\dagger + \text{diag}(V_{eff}, 0, 0), \quad (41)$$

with

$$H_0^d = \frac{1}{2E_\nu} \text{diag}(-\Delta m^2_{21}, 0, \Delta m^2_{32}). \quad (42)$$

with the same potential V_{eff} given for two-neutrino mixing subsection and U the three neutrino mixing matrix given by Gonzalez-Garcia & Nir (2003); Akhmedov et al. (2004); Gonzalez-Garcia & Maltoni (2008); Gonzalez-Garcia (2011)

$$U = \begin{pmatrix} c_{13}c_{12} & s_{12}c_{13} & s_{13} \\ -s_{12}c_{23} - s_{23}s_{13}c_{12} & c_{23}c_{12} - s_{23}s_{13}s_{12} & s_{23}c_{13} \\ s_{23}s_{12} - s_{13}c_{23}c_{12} & -s_{23}c_{12} - s_{13}s_{12}c_{23} & c_{23}c_{13} \end{pmatrix}, \quad (43)$$

where $s_{ij} = \sin \theta_{ij}$ and $c_{ij} = \cos \theta_{ij}$ and we have taken the Dirac phase $\delta = 0$. For anti-neutrinos one has to replace U by U^* . The different neutrino probabilities are given as

$$\begin{aligned} P_{ee} &= 1 - 4s_{13,m}^2 c_{13,m}^2 s_{31}, \\ P_{\mu\mu} &= 1 - 4s_{13,m}^2 c_{13,m}^2 s_{23}^4 s_{31} - 4s_{13,m}^2 s_{23}^2 c_{23}^2 s_{21} - 4c_{13,m}^2 s_{23}^2 c_{23}^2 s_{32}, \\ P_{\tau\tau} &= 1 - 4s_{13,m}^2 c_{13,m}^2 c_{23}^4 s_{31} - 4s_{13,m}^2 s_{23}^2 c_{23}^2 s_{21} - 4c_{13,m}^2 s_{23}^2 c_{23}^2 s_{32}, \\ P_{e\mu} &= 4s_{13,m}^2 c_{13,m}^2 s_{23}^2 s_{31}, \\ P_{e\tau} &= 4s_{13,m}^2 c_{13,m}^2 c_{23}^2 s_{31}, \\ P_{\mu\tau} &= -4s_{13,m}^2 c_{13,m}^2 s_{23}^2 c_{23}^2 s_{31} + 4s_{13,m}^2 s_{23}^2 c_{23}^2 s_{21} + 4c_{13,m}^2 s_{23}^2 c_{23}^2 s_{32}, \end{aligned} \quad (44)$$

where

$$\sin 2\theta_{13,m} = \frac{\sin 2\theta_{13}}{\sqrt{(\cos 2\theta_{13} - 2E_\nu V_e / \delta m_{32}^2)^2 + (\sin 2\theta_{13})^2}}, \quad (45)$$

and

$$S_{ij} = \sin^2 \left(\frac{\Delta \mu_{ij}^2}{4E_\nu} L \right). \quad (46)$$

Here $\Delta \mu_{ij}^2$ are given by

$$\begin{aligned} \Delta \mu_{21}^2 &= \frac{\Delta m_{32}^2}{2} \left(\frac{\sin 2\theta_{13}}{\sin 2\theta_{13,m}} - 1 \right) - E_\nu V_e, \\ \Delta \mu_{32}^2 &= \frac{\Delta m_{32}^2}{2} \left(\frac{\sin 2\theta_{13}}{\sin 2\theta_{13,m}} + 1 \right) + E_\nu V_e, \\ \Delta \mu_{31}^2 &= \Delta m_{32}^2 \frac{\sin 2\theta_{13}}{\sin 2\theta_{13,m}}, \end{aligned} \quad (47)$$

where

$$\begin{aligned} \sin^2 \theta_{13,m} &= \frac{1}{2} \left(1 - \sqrt{1 - \sin^2 2\theta_{13,m}} \right), \\ \cos^2 \theta_{13,m} &= \frac{1}{2} \left(1 + \sqrt{1 - \sin^2 2\theta_{13,m}} \right). \end{aligned} \quad (48)$$

The oscillation length for the neutrino is given by

$$L_{osc} = \frac{L_\nu}{\sqrt{\cos^2 2\theta_{13} \left(1 - \frac{2E_\nu V_e}{\delta m_{32}^2 \cos 2\theta_{13}} \right)^2 + \sin^2 2\theta_{13}}}, \quad (49)$$

where $L_\nu = 4\pi E_\nu / \delta m_{32}^2$ is the vacuum oscillation length. From the resonance condition, $\sqrt{2} G_F N_e = \Delta \cos 2\theta_{13}$, the resonance length and density are related as

$$\rho_R = \frac{1.9 \times 10^{-2}}{E_{\nu,TeV}} \left[1 - E_{\nu,TeV}^2 \left(\frac{8.2 \times 10^{10} \text{ cm}}{l_r} \right)^2 \right]^{1/2} \text{ gr/cm}^3. \quad (50)$$

On the other hand, generalizing the adiabaticity parameter, γ , to three-mixing neutrinos, it can be written as

$$\gamma \equiv \frac{\delta m_{32}^2}{2E} \sin 2\theta_{13} \tan 2\theta_{13} \frac{1}{\left| \frac{1}{p} \frac{dp}{dr} \right|_R}, \quad (51)$$

with the flip probability given by eq. (38).

5.2 Neutrino Oscillation from Source to Earth

Between the surface of the star and the Earth the flavor ratio $\phi_{\nu_e}^0 : \phi_{\nu_\mu}^0 : \phi_{\nu_\tau}^0$ is affected by the full three description flavor mixing, which is calculated as follow. The probability for a neutrino to oscillate from a flavor estate α to a flavor state β in a time starting from the emission of neutrino at star $t=0$, is given as

$$\begin{aligned} P_{\nu_\alpha \rightarrow \nu_\beta} &= |\langle \nu_\beta(t) | \nu_\alpha(t=0) \rangle| \\ &= \delta_{\alpha\beta} - 4 \sum_{j>i} U_{\alpha i} U_{\beta i} U_{\alpha j} U_{\beta j} \sin^2 \left(\frac{\delta m_{ij}^2 L}{4E_\nu} \right) \end{aligned} \quad (52)$$

Using the set of parameters give in eq. (29), we can write the mixing matrix

$$U = \begin{pmatrix} 0.816669 & 0.544650 & 0.190809 \\ -0.504583 & 0.513419 & 0.694115 \\ 0.280085 & -0.663141 & 0.694115 \end{pmatrix}. \quad (53)$$

Averaging the sin term in the probability to ~ 0.5 for larger distances L (Learned & Pakvasa 1995), the probability matrix for a neutrino flavor vector of $(\nu_e, \nu_\mu, \nu_\tau)_{source}$ changing to a flavor vector $(\nu_e, \nu_\mu, \nu_\tau)_{Earth}$ is given as

$$\begin{pmatrix} \nu_e \\ \nu_\mu \\ \nu_\tau \end{pmatrix}_{Earth} = \begin{pmatrix} 0.534143 & 0.265544 & 0.200313 \\ 0.265544 & 0.366436 & 0.368020 \\ 0.200313 & 0.368020 & 0.431667 \end{pmatrix} \begin{pmatrix} \nu_e \\ \nu_\mu \\ \nu_\tau \end{pmatrix}_{source} \quad (54)$$

for distances longer than the solar system.

6 RESULTS AND DISCUSSIONS

We have considered a core collapse of massive stars leading to supernovae (SNe) of type Ib,c and II with mildly relativistic jets. Although this mildly relativistic jet may not be able to break through the stellar envelope, electrons and protons are expected to be accelerated in the internal shocks, and then to be cooled down by synchrotron radiation, inverse Compton and hadronic processes ($p\gamma$ and p -hadron/meson). Photons from electron synchrotron radiation thermalized to a some keV-peak energy serve as cooling mechanism for accelerated protons by means of $p\gamma$ interactions. Another cooling mechanism of protons considered here are the p - p interactions, due to the high number density of protons ($3.1 \times 10^{20} \text{ cm}^{-3} \leq n_p' \leq 3.1 \times 10^{22} \text{ cm}^{-3}$) (Razzaque, Mészáros & Waxman 2005). In $p\gamma$ and p - p interactions, high-energy pions and kaons are created which in turn interact with protons by π - p and K - p interactions, producing another hadronic/meson cooling mechanism. To illustrate the degree and energy region of efficiency of each cooling process, we have plotted the proton (figures 1 and 2) and meson (figures 3 and 4) time scales when internal shocks take place at $6 \times 10^9 \text{ cm}$ and $6 \times 10^{10} \text{ cm}$ and, the magnetic field lies in the range $3.4 \times 10^7 \text{ G} \leq B' \leq 1.1 \times 10^{10} \text{ G}$. Comparing the time scales in figures 1 and 2, one can observe that the maximum proton energy is when the acceleration and synchrotron time scales are equal; it happens when proton energy is in the range $10^{15} \text{ eV} \leq E_p' \leq 10^{16} \text{ eV}$ which corresponds to internal shocks at $6 \times 10^9 \text{ cm}$ with $B' = 1.1 \times 10^{10} \text{ G}$ and $6 \times 10^{10} \text{ cm}$ with $B' = 3.4 \times 10^7 \text{ G}$, respectively. In figs. 3 and 4, one can see that hadronic time scales are equal to other time scales at different energies. For instance, internal shocks at $6 \times 10^{10} \text{ cm}$ and $B' = 1.1 \times 10^9 \text{ G}$, the time scales of pion synchrotron emission and hadronic are equal for pion energy $\sim 5 \times 10^{11} \text{ eV}$. Computing the break meson energies for which time scales are equal to each other, we can estimate the break neutrino energies. From the equality of kaon/pion lifetime and synchrotron cooling time scales we obtain the break neutrino energies $\sim (24/179) \text{ GeV}$ and $\sim 428 \text{ GeV}/69 \text{ TeV}$, respectively. Also, considering $p\gamma$ interactions the threshold neutrino energy $\sim 3 \text{ TeV}$ is obtained. Taking into account the distances of internal shocks ($6 \times 10^9 \text{ cm}$ and $6 \times 10^{10} \text{ cm}$) we have plotted the neutrino energy as a function of the magnetic equipartition parameter in the range $0.1 \leq \epsilon_B \leq 10^{-4}$ ($3.4 \times 10^7 \text{ G} \leq B' \leq 1.1 \times 10^{10} \text{ G}$). As shown in the fig. 5, neutrino energy between 1 - 10 PeV can be generated for ϵ_B between 3.5×10^{-3} and 4.1×10^{-4} , that corresponds to a magnetic field in the range 2.02×10^8 (2.02×10^9) G - 6.9×10^7 (6.9×10^8) G at $6 \times 10^9 \text{ cm}$ and $6 \times 10^{10} \text{ cm}$ from the central engine, respectively. Under this scenario, choked jets are bright in high-energy neutrinos and dark in gamma rays.

On the other hand, taking into account the range of neutrino energy ($24 \text{ GeV} \leq E_\nu \leq 69 \text{ TeV}$), internal shocks at a distance of $6 \times 10^{10} \text{ cm}$, strength of magnetic field of $1.1 \times 10^{10} \text{ G}$ and considering three models of density profile (see section III. eqs. 25, 26 and 27) of a pre-supernova star, we present a full description of two- and three-flavor neutrino oscillations. Based on these models of density profiles we calculate the effective potential, the resonance condition and, the resonance length and density. From the

resonance condition, we obtain the resonance density (ρ_R) as a function of resonance length (l_R) for two (eq. 36) and three flavors (eq. 50). We overlap the plots of the density profiles as a function of distance with the resonance conditions (resonance density as a function of resonance length). They are shown in Fig 7 (two flavors) and in Fig. 6 (three flavors). For two flavors, we have taken into account solar (top), atmospheric (middle) and accelerator (bottom) parameters of neutrino experiments. Using solar parameters, the resonance length is in the range $\sim (10^{11} - 10^{14.2})$ cm and resonance density in $\sim (10^{-2} - 10^{-4})\text{g/cm}^3$. As can be seen, neutrinos with energy 24 GeV are the only ones that meet the resonance condition for all models of density profiles while neutrinos of energy 178 GeV meet marginally the resonance condition just for the model [B]. Neutrinos with other energy cannot meet the resonance condition. Using atmospheric parameters, the resonance length lies in the range $\sim (10^{9.1} - 10^{13.3})$ cm and the resonance density in $\sim (10^1 - 10^{-4})\text{g/cm}^3$. As shown, neutrinos in the energy range of 178 GeV - 3 TeV can oscillate many times before leaving the source. Although the resonance length of neutrino with energy 24 GeV is smaller than star radius, the resonance density is greater than other models. Using accelerator parameters, the resonance length is less than $\sim 10^{10.2}$ cm and the resonance density lies in the range $\sim (10^2 - 10^2)\text{g/cm}^3$. Although the resonance length is smaller than the star radius for two flavors, the one that meets the resonance density is the neutrino energy 69 TeV. For three flavors, the range of resonance length is $\sim (10^9 - 10^{12.5})$ cm and resonance density is $\sim (0.9 - 10^{-4})\text{g/cm}^3$, presenting a similar behavior to that described by means of atmospheric parameters. As the dynamics of resonant transitions is not only determined by the resonance condition, but also by adiabatic conversion, we plot the flip probability as a function of neutrino energy for two (fig 8) and three flavors (fig 9). Dividing the plots of flip probabilities in three regions of less than 0.2, between 0.2 and 0.8 and greater than 0.8, we have that in the first case ($P_\gamma \leq 0.2$), a pure adiabatic conversion occurs, the last case ($P_\gamma \geq 0.8$) is a strong violation of adiabaticity and the intermediate region $0.2 < P_\gamma < 0.8$ represents the transition region (Dighe & Smirnov 2000). In Fig. 8, the top, middle and bottom plots are obtained using solar, atmospheric and accelerator parameters of neutrino oscillations, respectively. As shown in top figure, the pure adiabatic conversion occurs when neutrino energy is less than 5×10^{11} eV for model [A] and [C] and, $\sim 10^{12}$ eV for model [B] and, the strong violation of adiabaticity is given for neutrino energy greater than 6×10^{12} eV in the three profiles. In the middle figure, one can see that independently of the profile, neutrinos with energy of less than $E_\nu=10^{14}$ eV can have pure adiabatic conversions. In the bottom figure, the three models of density profiles have the same behavior for the whole energy range. Neutrinos with energy less than $\sim 10^{11.3}$ eV and greater than $\sim 10^{13.2}$ eV present conversion adiabatically pure and strong violation, respectively. In fig. 9, the flip probability for three flavors are plotted. The energy range for each region of P_γ changes marginally according to the model of density profile. Neutrinos with $E \sim 10^{12}$ eV are capable of having pure adiabatic conversion in [B] but not in [A] or [C]. The strong violation of adiabaticity begins when the neutrino energies are $E \sim 10^{13}$ eV and $E \sim 10^{13.8}$ eV, for [A] and [C], respectively.

On the other hand, we have also plotted (fig. 10) the oscillation probabilities for three flavors as a function of energy when neutrinos keep moving at a distance of $r=10^{11}$ cm (above) and $r=10^{12}$ cm (below) from the core. In the top figure, the survival probability of electron neutrino, P_{ee} , is close to one regardless of neutrino energy, therefore the conversion probabilities $P_{\mu e}$ and $P_{\tau e}$ are close to zero,

E_ν (TeV)	$\phi_{\nu e} : \phi_{\nu\mu} : \phi_{\nu\tau}$ ($L=10^{11}$ cm)	$\phi_{\nu e} : \phi_{\nu\mu} : \phi_{\nu\tau}$ ($L=10^{11.5}$ cm)	$\phi_{\nu e} : \phi_{\nu\mu} : \phi_{\nu\tau}$ ($L=10^{12}$ cm)
0.024	0.946:1.949:0.115	0.697:1.405:0.899	0.881:1.578:0.541
0.178	0.510:1.814:0.676	0.987:1.386:0.627	0.507:1.807:0.686
0.428	0.983:1.589:0.428	0.659:1.871:0.524	0.538:1.721:0.741
3	0.896:1.212:0.892	0.502:1.753:0.744	0.501:1.762:0.737
68.5	0.999:1.997:0.003	0.998:1.972:0.030	0.979:1.746:0.275

Table 1. The flavor ratio on the surface of source for five neutrino energies ($E_\nu=24$ GeV, 178 GeV, 428 GeV, 3 TeV and 68.5 TeV), leaving the star to three distances $L=10^{11}$ cm, $10^{11.5}$ cm, and 10^{12} cm.

as shown. Depending on the neutrino energy, the survival probability of muon and tau neutrino, $P_{\mu\mu}$ and $P_{\tau\tau}$, oscillates between zero and one. For example, for $E \sim 430$ GeV, the conversion probability of muon $P_{\mu\tau}$ is close to zero while the survival probability of muon and tau neutrino, $P_{\mu\mu}$ and $P_{\tau\tau}$, are close to one, and for $E \sim 1$ TeV probabilities change dramatically, being $P_{\mu\tau} \sim 1$ and $P_{\tau\tau}=P_{\mu\mu} \sim 0$. In the bottom figure, neutrinos are moving along the jet at $r=10^{12}$ cm and although the survival and conversion probabilities have similar behaviors to those moving to $r=10^{11}$ cm, they are changing faster. To have a better understanding, we have separated all probabilities and plotted them in fig. 11. From up to down, the probabilities of electron neutrino and survival probability of muon neutrino are shown in the first and second graph, respectively, and the conversion and survival probability of tau neutrino are plotted in the third and four graph, respectively. Moreover, we have plotted in figs. 12 and 13 the oscillation probabilities as a function of distance, when neutrinos are produced at a radius 6×10^9 cm and 6×10^{10} cm, respectively, and continue to propagate along the jet. We take into account four neutrino energies $E_\nu=178$ GeV, $E_\nu=428$ GeV, $E_\nu=3$ TeV and $E_\nu=69$ TeV. As shown, as neutrino energy increases, the probabilities oscillate less. For instance, when an electron neutrino with energy $E_\nu=178$ GeV propagates along the jet, the survival probability of electron changes from one at $\sim 8 \times 10^{10}$ cm to zero at $\sim 9.5 \times 10^{10}$ cm. For $E_\nu=428$ GeV (3 TeV), the survival probabilities change from one at 9.1×10^{10} (6.0×10^{10}) cm to zero at 1.8×10^{11} (3.5×10^{11}) cm and for $E_\nu=69$ TeV, the probability is constant in this range (greater than $\sim 10^{12}$ cm). In the last case, neutrino does not oscillate to another flavor during its propagation. Finally, considering a flux ratio for π , K and μ decay of 1: 2: 0, the density profile [A] and oscillation probabilities at three distances (10^{11} cm, $10^{11.5}$ cm and 10^{12} cm), we show in table 1 the flavor ratio on the surface of star. Also, computing the vacuum oscillation effects between the source and Earth (Eq. 54), we estimate and show in table 2 the flavor ratio expected on Earth when neutrinos emerge from the star at $L=(10^{11}, 10^{11.5}$ and $10^{12})$ cm.

7 SUMMARY AND CONCLUSIONS

We have done a wide description of production channels of high-energy neutrinos in a middle relativistic hidden jet and also shown that neutrinos with energies between 1 - 10 PeV can be generated. Taking into account a particular range of neutrino energies generated in the internal shocks at a distance of 6×10^{10} cm and with a distribution of magnetic field 1.1×10^{10} G, we have shown their oscillations between flavors along the jet for three models of den-

E_ν (TeV)	$\phi_{\nu_e}^0 : \phi_{\nu_\mu}^0 : \phi_{\nu_\tau}^0$ ($L=10^{11}$ cm)	$\phi_{\nu_e}^0 : \phi_{\nu_\mu}^0 : \phi_{\nu_\tau}^0$ ($L=10^{11.5}$ cm)	$\phi_{\nu_e}^0 : \phi_{\nu_\mu}^0 : \phi_{\nu_\tau}^0$ ($L=10^{12}$ cm)
0.024	1.046:1.008:0.956	0.925:1.031:1.045	0.998:1.011:0.991
0.178	0.889:1.049:1.062	1.021:1.000:0.978	0.888:1.049:1.063
0.428	1.033:1.000:0.966	0.954:1.053:1.047	0.893:1.046:1.061
3	0.979:1.010:1.011	0.883:1.049:1.067	0.883:1.050:1.067
68.5	1.065:0.998:0.936	1.063:0.999:0.939	1.042:1.001:0.957

Table 2. The flavor ratio expected on Earth for five neutrino energies ($E_\nu=24$ GeV, 178 GeV, 428 GeV, 3 TeV and 68.5 TeV), leaving the star to three distances $L=10^{11}$ cm, $10^{11.5}$ cm, and 10^{12} cm.

sity profiles. For two neutrinos mixing, we have used the fit values of neutrino oscillation parameters from solar, atmospheric, and accelerator experiments and analyzing the resonance condition we found that the resonance lengths are the largest and resonance densities are the smallest for solar parameters and using accelerator parameters we have obtained the opposite situation, the resonance lengths are the smallest and resonance densities are the largest. The most favorable condition for high-energy neutrinos to oscillate resonantly before going out of the source is given through atmospheric parameters and these conversions would be pure adiabatic. For three neutrino mixing, we have calculated the ratio flavor on the surface of the source as well as that expected on Earth. Our analysis shows that deviations from 1:1:1 are obtained at different energies and places along the jet, which is given in table 2. From analysis of flip probability we also show that neutrinos may oscillate depending on their energy and the parameters of neutrino experiments. As a particular case, when the three-flavor parameters are considered (fig. 9), we obtain that neutrino energies above ≥ 10 TeV can hardly oscillate, obtaining the same result given by Osorio Oliveros, Sahu & Sanabria (2013).

As shown, depending on the flavor ratio obtained on Earth we could differentiate the progenitor, its density profile at different depths in the source, as well as understand similar features between IGRBs and core collapse supernovae. Distinct times of arrival of neutrino flavor ratio will provide constraints on density profiles at different places in the star (Bartos, Dasgupta & Márka 2012). These observations in detectors such as IceCube, Antares and KM3Net would be a compelling evidence that choked jets are bright in neutrinos (Abbasi et al. 2007; IceCube Collaboration et al. 2013b; Pradier & Antares Collaboration 2010; Leisos et al. 2012). The number of sources with hidden jets may be much larger than the exhibited one, limited only by the ratio of type Ib/c and type II SNe to GRB rates. Within 10 Mpc, the rate of core-collapse supernovae is $\sim 1 - 3 \text{ yr}^{-1}$, with a large contribution of galaxies around 3 - 4 Mpc. At larger distances, the expected number of neutrino events in IceCube is still several, and the supernova rate is $\geq 10 \text{ yr}^{-1}$ at 20 Mpc (Ando & Beacom 2005). Recently, Taboada (2010) calculated the events expected in DeepCore and neutrino-induced cascades in km^3 detectors for neutrinos energies ≤ 10 GeV and \leq a few TeV respectively and forecast that ~ 4 events in DeepCore and ~ 6 neutrino-induced cascades in IceCube/KM3Net would be expected. An extension up to higher energies of this calculation should be done to correlate the expected events in these sources with the number of PeV-neutrinos observed with IceCube (IceCube Collaboration et al. 2013a).

Interference effects in the detector by atmospheric neutrino os-

cillation are very small (less than 10 %) due to short path traveled by neutrinos in comparison with cosmological distances (Mena, Mocioiu & Razzaque 2007).

ACKNOWLEDGEMENTS

We thank the referee for a critical reading of the paper and valuable suggestions. We also thank B. Zhang, K. Murase, William H. Lee, Fabio de Colle, Enrique Moreno and Antonio Marinelli for useful discussions. NF gratefully acknowledges a Luc Binette-Fundación UNAM Posdoctoral Fellowship.

REFERENCES

- Abbasi R. et al., 2012, *Astroparticle Physics*, 35, 615
Abe K., et al., 2011, *Physical Review Letters*, 107, 241801
Aguilar-Arevalo A. A., et al., 2007, *Physical Review Letters*, 98, 231801
Aguilar-Arevalo A. A., et al., 2009, *Physical Review Letters*, 102, 101802
Aguilar-Arevalo A. A., et al., 2010, *Physical Review Letters*, 105, 181801
Aharmim B., et al., 2011, *ArXiv e-prints*
Ahn M. H., et al., 2006, *Phys. Rev. D*, 74, 072003
Akhmedov E. K., Johansson R., Lindner M., Ohlsson T., Schwetz T., 2004, *Journal of High Energy Physics*, 4, 78
Alvarez-Muñiz J., Halzen F., 2002, *ApJ*, 576, L33
Alvarez-Muñiz J., Mészáros P., 2004, *Phys. Rev. D*, 70, 123001
Ando S., Beacom J. F., 2005, *Physical Review Letters*, 95, 061103
Araki T., et al., 2005, *Physical Review Letters*, 94, 081801
Armbruster B., et al., 2002, *Phys. Rev. D*, 65, 112001
Arnett D., 1991, *ApJ*, 383, 295
Athanassopoulos C., et al., 1996, *Physical Review Letters*, 77, 3082
Athanassopoulos C., et al., 1998, *Physical Review Letters*, 81, 1774
Athar H., Jeżabek M., Yasuda O., 2000, *Phys. Rev. D*, 62, 103007
Atoyan A., Dermer C. D., 2001, *Physical Review Letters*, 87, 221102
Barniol Duran R., Bošnjak Ž., Kumar P., 2012, *MNRAS*, 424, 3192
Bartos I., Dasgupta B., Márka S., 2012, *Phys. Rev. D*, 86, 083007
Becker J. K., Biermann P. L., 2009, *Astroparticle Physics*, 31, 138
Bethe H. A., Pizzochero P., 1990, *ApJ*, 350, L33
Chen H. H., 1985, *Physical Review Letters*, 55, 1534
Chevalier R. A., Soker N., 1989, *ApJ*, 341, 867
Cholis I., Hooper D., 2012, *ArXiv e-prints*
Church E. D., Eitel K., Mills G. B., Steidl M., 2002, *Phys. Rev. D*, 66, 013001
Costantini M. L., Vissani F., 2005, *Astroparticle Physics*, 23, 477
Dermer C. D., Atoyan A., 2003, *Physical Review Letters*, 91, 071102
Dermer C. D., Menon G., 2009, *High Energy Radiation from Black Holes: Gamma Rays, Cosmic Rays, and Neutrinos*
Dighe A. S., Smirnov A. Y., 2000, *Phys. Rev. D*, 62, 033007
Fraija N., González M. M., Lee W. H., 2012, *ApJ*, 751, 33
Gonzalez-Garcia M. C., 2011, *Physics of Particles and Nuclei*, 42, 577
Gonzalez-Garcia M. C., Maltoni M., 2008, *Phys. Rep.*, 460, 1
Gonzalez-Garcia M. C., Nir Y., 2003, *Reviews of Modern Physics*, 75, 345

- Gupta N., Zhang B., 2007, *Astroparticle Physics*, 27, 386
- Hjorth J., et al., 2003, *Nature*, 423, 847
- IceCube Collaboration et al., 2013a, ArXiv e-prints
- IceCube Collaboration et al., 2013b, *ApJ*, 763, 33
- Kashti T., Waxman E., 2005, *Physical Review Letters*, 95, 181101
- Kumar P., Barniol Duran R., 2010, *MNRAS*, 409, 226
- Kuo T. K., Pantaleone J., 1989, *Reviews of Modern Physics*, 61, 937
- Learned J. G., Pakvasa S., 1995, *Astroparticle Physics*, 3, 267
- Leisos A., Tsirigotis A. G., Tzamarias S. E., KM3NeT consortium f. t., 2012, ArXiv e-prints
- Liu R.-Y., Wang X.-Y., 2013, *ApJ*, 766, 73
- MacLachlan G. A. et al., 2013, *MNRAS*, 432, 857
- Matzner C. D., McKee C. F., 1999, *ApJ*, 510, 379
- Mena O., Mocioiu I., Razzaque S., 2007, *Phys. Rev. D*, 75, 063003
- Meszáros P., Rees M. J., Wijers R. A. M. J., 1998, *ApJ*, 499, 301
- Murase K., Ioka K., Nagataki S., Nakamura T., 2006, *ApJ*, 651, L5
- Nellen L., Mannheim K., Biermann P., 1993, *Phys. Rev. D*, 47, 5270
- Osorio Oliveros A. F., Sahu S., Sanabria J. C., 2013, ArXiv e-prints
- Pradier T., Antares Collaboration, 2010, *Classical and Quantum Gravity*, 27, 194004
- Razzaque S., Mészáros P., Waxman E., 2004, *Physical Review Letters*, 93, 181101
- Razzaque S., Mészáros P., Waxman E., 2005, *Modern Physics Letters A*, 20, 2351
- Razzaque S., Smirnov A. Y., 2010, *Journal of High Energy Physics*, 3, 31
- Sacahui J. R., Fraija N., González M. M., Lee W. H., 2012, *ApJ*, 755, 127
- Sahu S., Zhang B., 2010, *Research in Astronomy and Astrophysics*, 10, 943
- Shen R., Kumar P., Piran T., 2010, *MNRAS*, 403, 229
- Shigeyama T., Nomoto K., 1990, *ApJ*, 360, 242
- Shirai J., KamLAND Collaboration, 2007, *Nuclear Physics B Proceedings Supplements*, 168, 77
- Stanek K. Z., et al., 2003, *ApJ*, 591, L17
- Stecker F. W., 1968, *Physical Review Letters*, 21, 1016
- Stecker F. W., Done C., Salamon M. H., Sommers P., 1991, *Physical Review Letters*, 66, 2697
- Szabo A. P., Protheroe R. J., 1994, *Astroparticle Physics*, 2, 375
- Taboada I., 2010, *Phys. Rev. D*, 81, 083011
- the KamLAND Collaboration, Mitsui T., 2011, *Nuclear Physics B Proceedings Supplements*, 221, 193
- Wang X.-Y., Razzaque S., Mészáros P., Dai Z.-G., 2007, *Phys. Rev. D*, 76, 083009
- Waxman E., Bahcall J., 1997, *Physical Review Letters*, 78, 2292
- Waxman E., Loeb A., 2001, *Physical Review Letters*, 87, 071101
- Wendell R., et al., 2010, *Phys. Rev. D*, 81, 092004
- Wolfenstein L., 1978, *Phys. Rev. D*, 17, 2369
- Woosley S. E., Langer N., Weaver T. A., 1993, *ApJ*, 411, 823

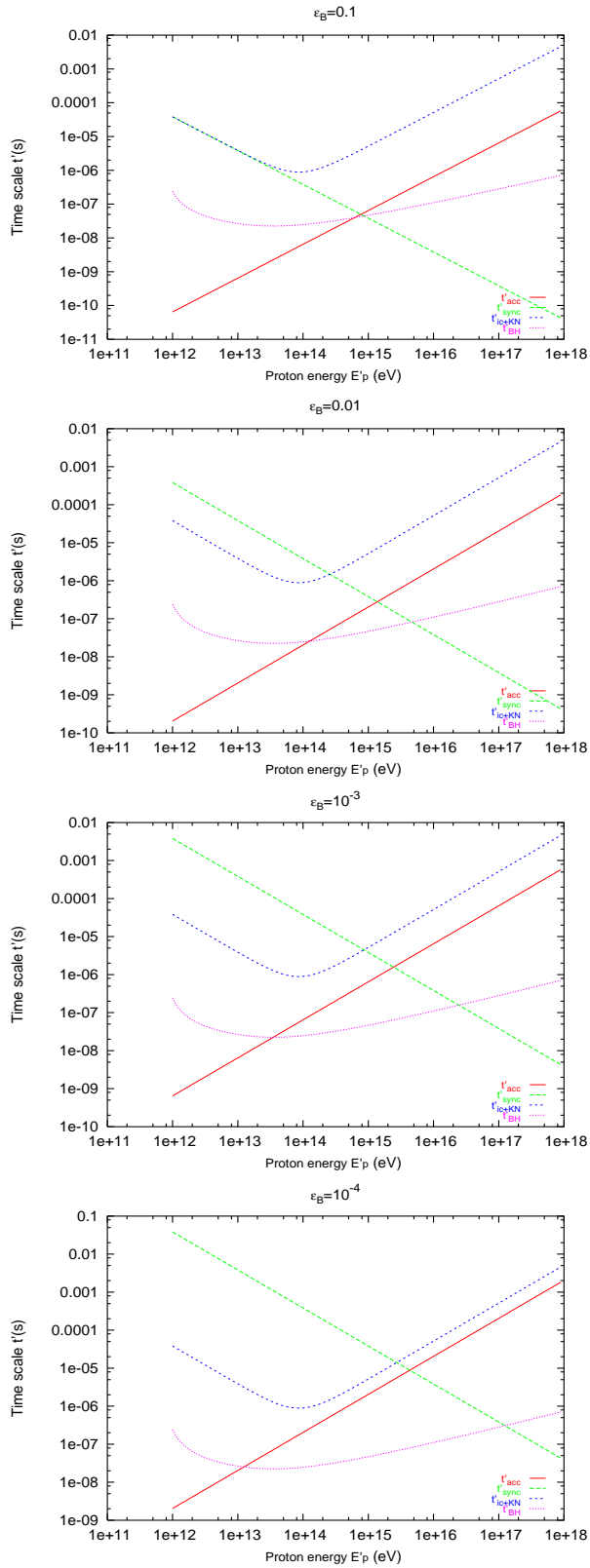


Figure 1. Proton cooling time scales in the comoving frame for different processes as a function of proton energy (E_p) when the shell collisions take place at $r=6 \times 10^9$ cm and different magnetic fields. Synchrotron radiation (t'_{sync}), IC+KN scattering (t'_{ic+KN}), Bethe-Heitler (t'_{BH}), shock acceleration time (t'_{acc}).

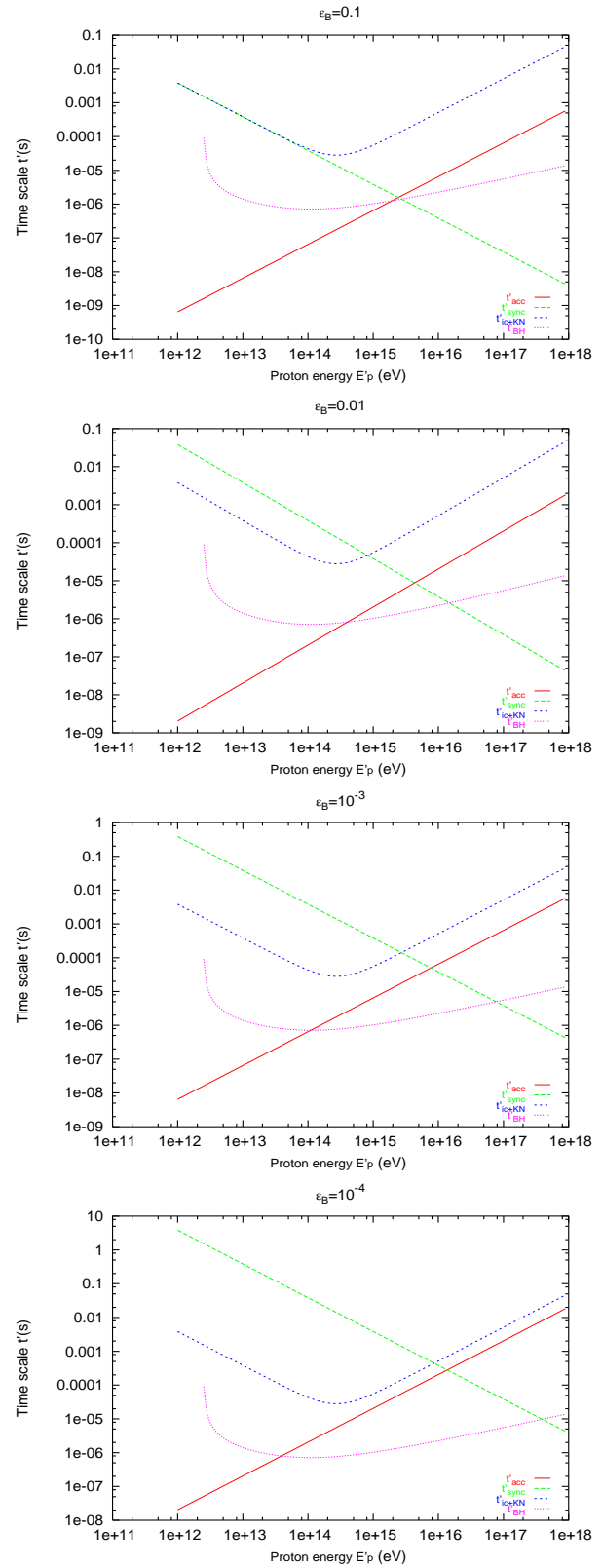


Figure 2. Proton cooling time scales in the comoving frame for different processes as a function of proton energy (E_p) when the shell collisions take place at $r=6 \times 10^{10}$ cm and different magnetic fields. Synchrotron radiation (t'_{sync}), IC+KN scattering (t'_{ic+KN}), Bethe-Heitler (t'_{BH}), shock acceleration time (t'_{acc}).

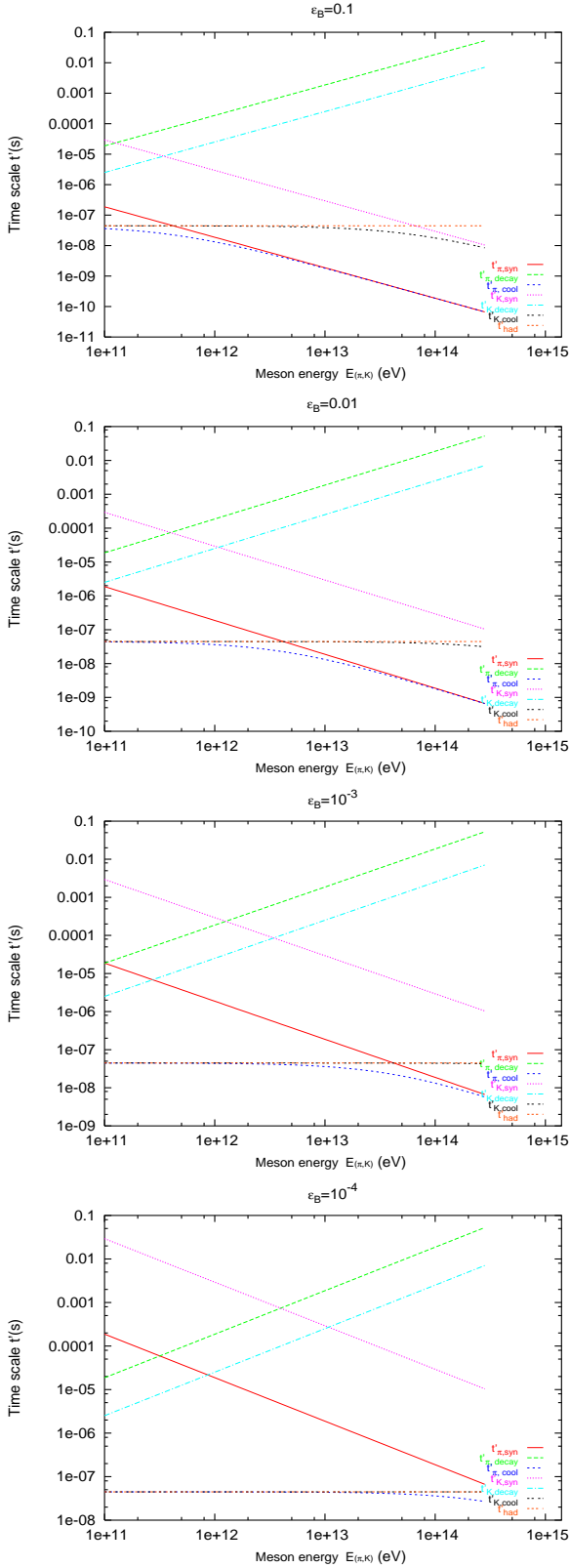


Figure 3. Meson (π^\pm/K^\pm) cooling time scales in the comoving frame for different processes as a function of Meson energy ($E_{\pi/K}$) when the shell collisions take place at $r=6 \times 10^9$ cm and different magnetic fields. π/K - synchrotron radiation ($t'_{(\pi/K), syn}$), π/K - decay ($t'_{(\pi/K), decay}$), π/K - synchrotron and hadronic radiation (t'_{cool}).

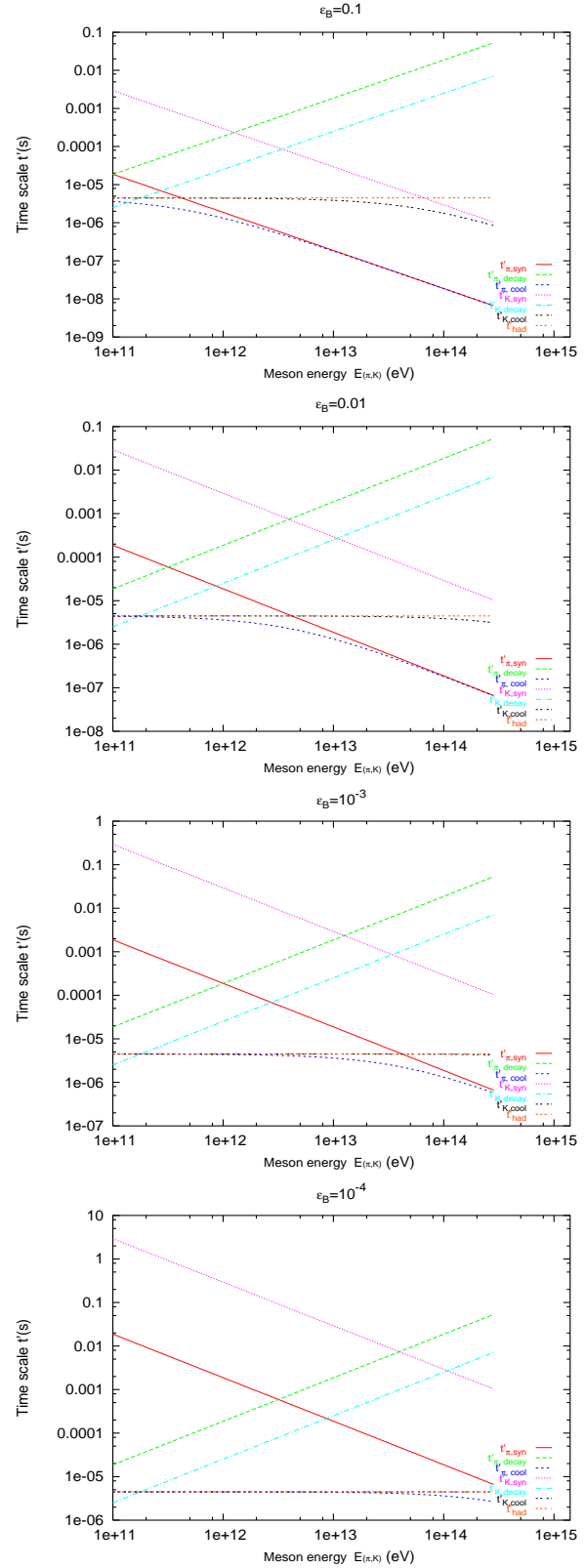


Figure 4. Meson (π^\pm/K^\pm) cooling time scales in the comoving frame for different processes as a function of Meson energy ($E_{\pi/K}$) when the shell collisions take place at $r=6 \times 10^{10}$ cm and different magnetic fields. π/K - synchrotron radiation ($t'_{(\pi/K), syn}$), π/K - decay ($t'_{(\pi/K), decay}$), π/K - synchrotron and hadronic radiation (t'_{cool}).

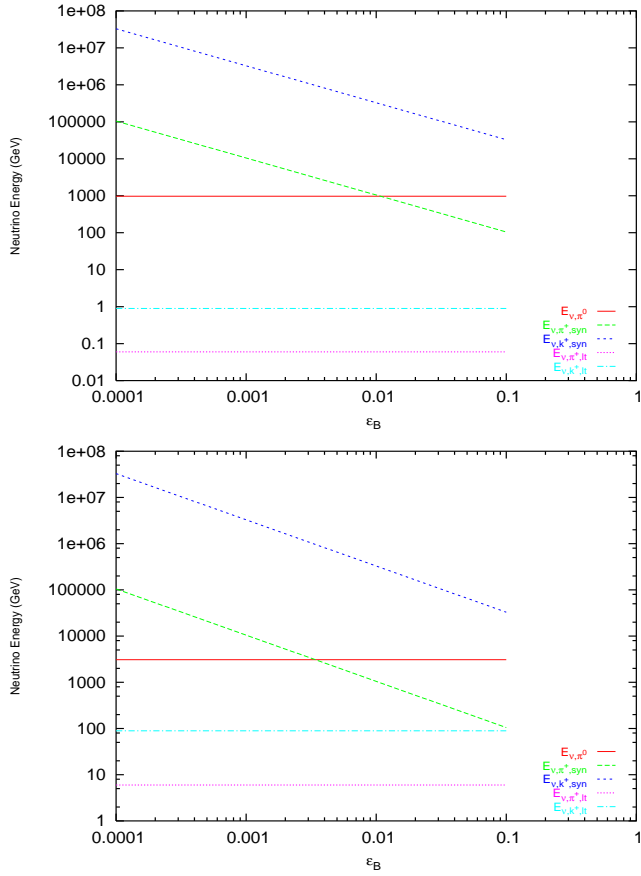


Figure 5. neutrino energy created at 6×10^9 cm (above) and 6×10^{10} cm (below) for different interaction processes as a function of magnetic equipartition parameter.

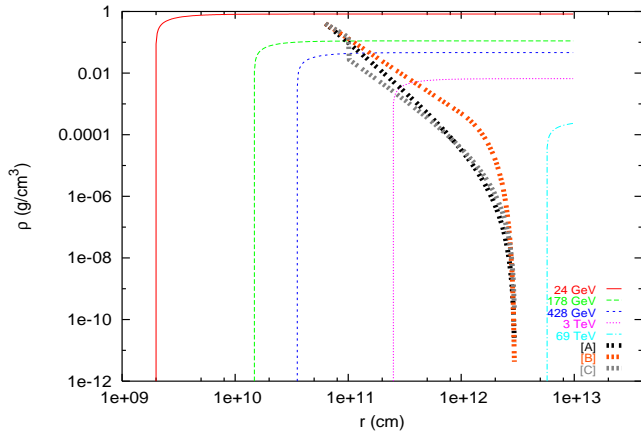


Figure 6. In the top figure, Density profiles ([A], [B] and [C]) given by eqs. (25), (26) and (27), respectively are plotted. Also from the resonance condition, we plot the resonance density as a function of resonance length for High-energy neutrinos. In the bottom figure, the flip probability is plotted as a function of neutrino energy for density profiles [A] (eq. 25), [B] (eq. 26) and [C] (eq. 27). We have used the best parameters of the three-flavor neutrino oscillation.

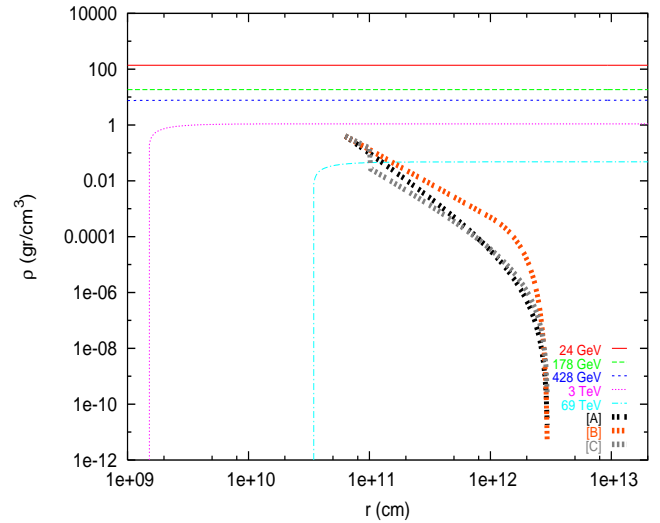
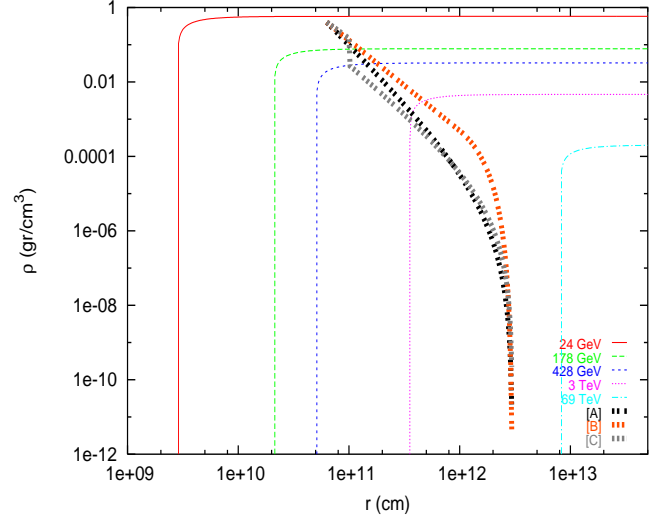
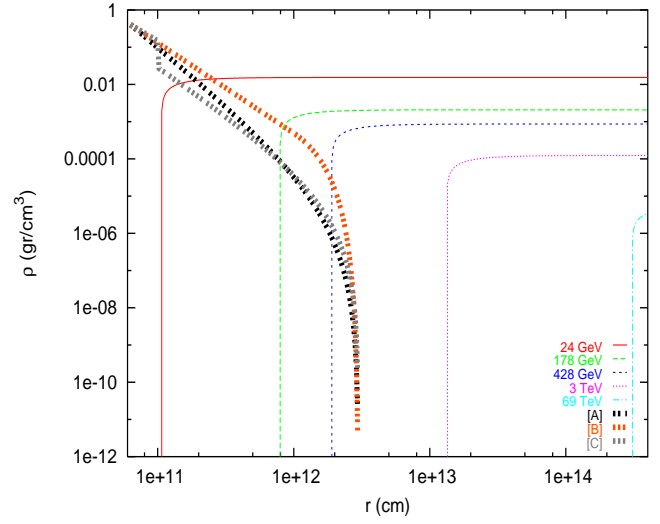


Figure 7. Density profiles ([A], [B] and [C]) given by eqs. (25), (26) and (27), respectively are plotted. Also from the resonance condition, we plot the resonance density as a function of resonance length for High-energy neutrinos. We have used the best parameters of the two-flavor solar (above), atmospheric (medium) and accelerator (below) neutrino oscillation.

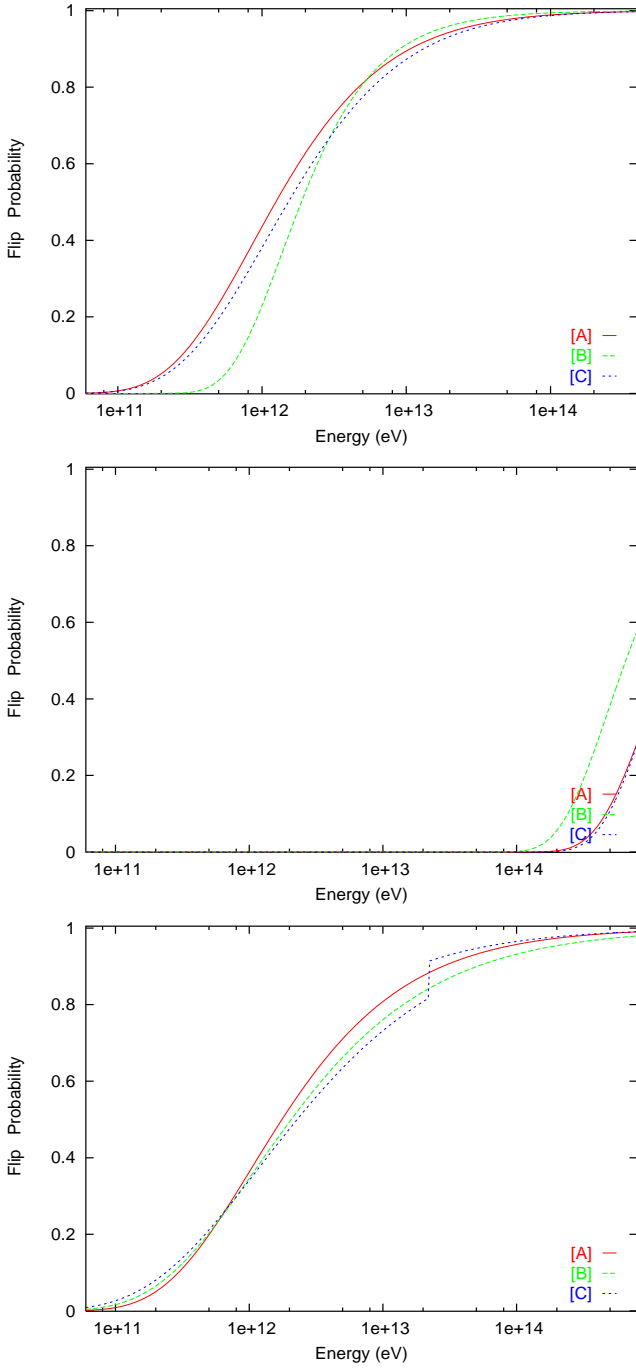


Figure 8. The flip probability is plotted as a function of neutrino energy for density profiles [A] (eq. 25), [B] (eq. 26) and [C] (eq. 27). On the top figure we use solar parameters, on the middle figure we use atmospheric parameters and on the bottom figure we use accelerator neutrinos.

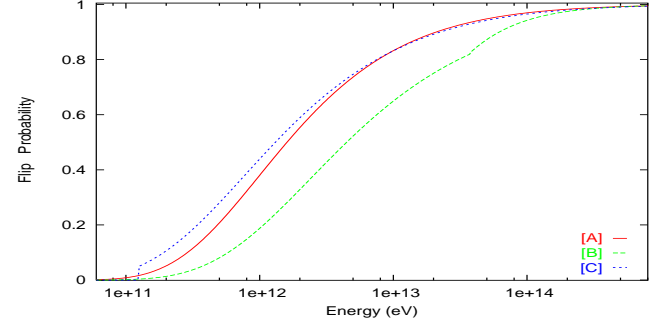


Figure 9. The flip probability is plotted as a function of neutrino energy for density profiles [A] (eq. 25), [B] (eq. 26) and [C] (eq. 27). We have used the best parameters of the three-flavor neutrino oscillation.

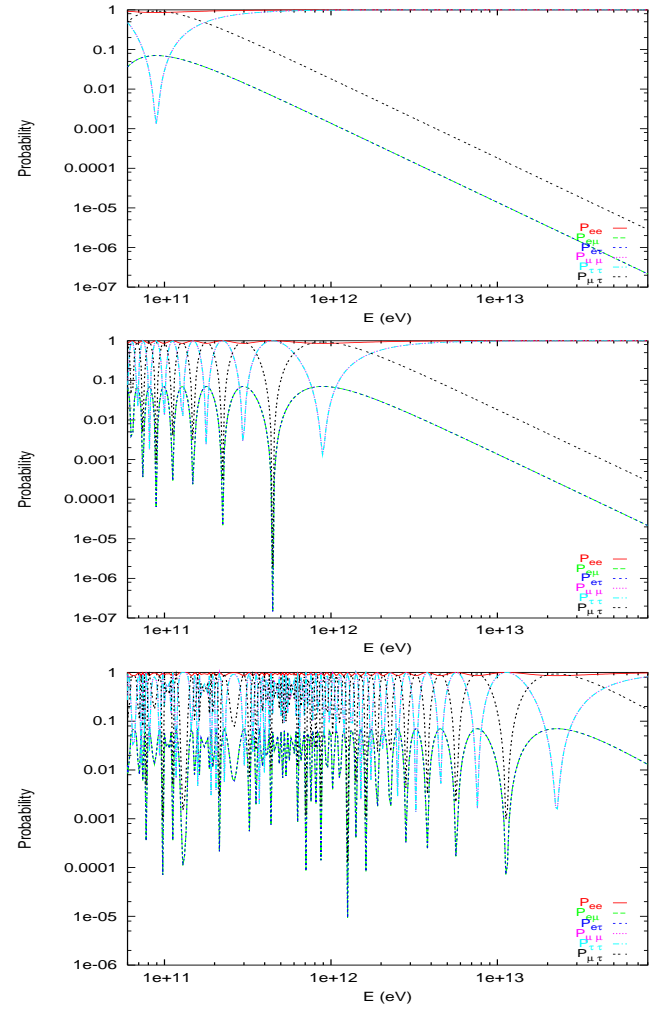


Figure 10. We have plotted the oscillation probability as a function of neutrino energy for neutrinos produced at radii $r = 6 \times 10^9$ cm and $r = 6 \times 10^{10}$ cm. In the top, middle and bottom figures we plot the oscillation probabilities when neutrinos are moving at $r = 10^{10}$ cm, $r = 10^{11}$ cm and $r = 10^{12}$ cm, respectively.

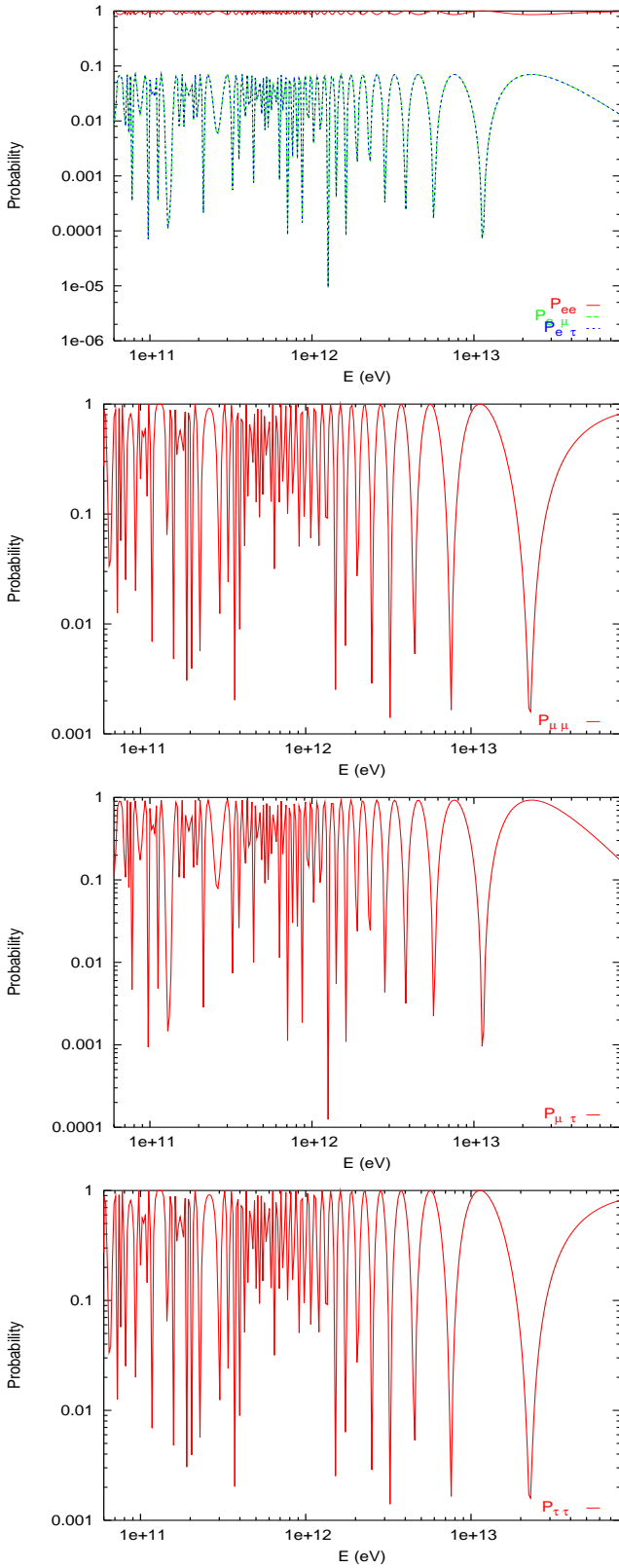


Figure 11. To have a better visibility of bottom figure 10, we separate the oscillation probabilities like, figures from up to down, P_{ei} for e, μ, τ (first one), $P_{\mu\mu}$ (second one), $P_{\mu\tau}$ (third one) and $P_{\tau\tau}$ (four one).

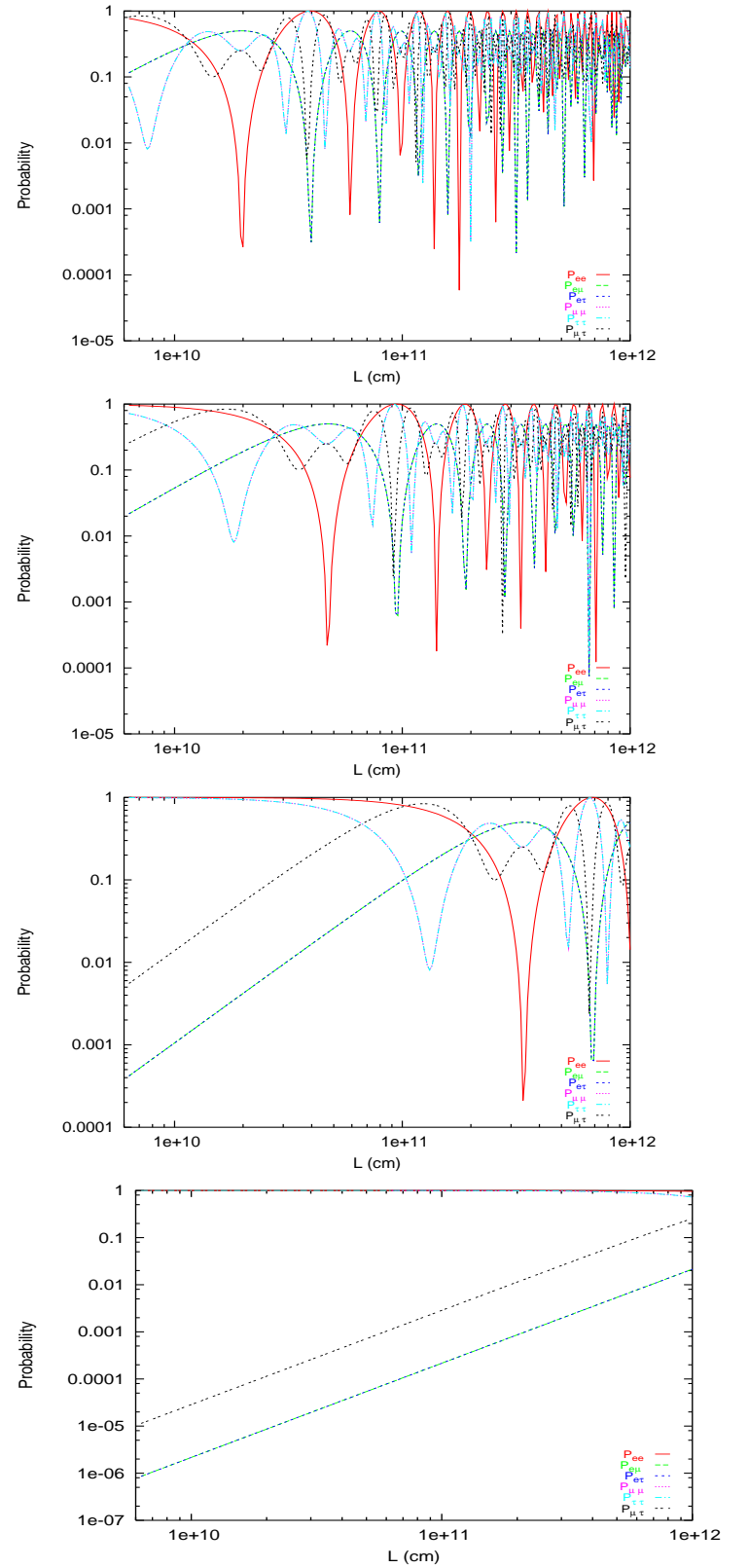


Figure 12. We plot the oscillation probability when neutrinos are produced at a radius $r = 6 \times 10^9$ cm and are propagating through the jet direction for four energies: $E_\nu = 178$ GeV (first figure), $E_\nu = 428$ GeV (second figure), $E_\nu = 3$ TeV (third figure) and $E_\nu = 69$ TeV (four figure)

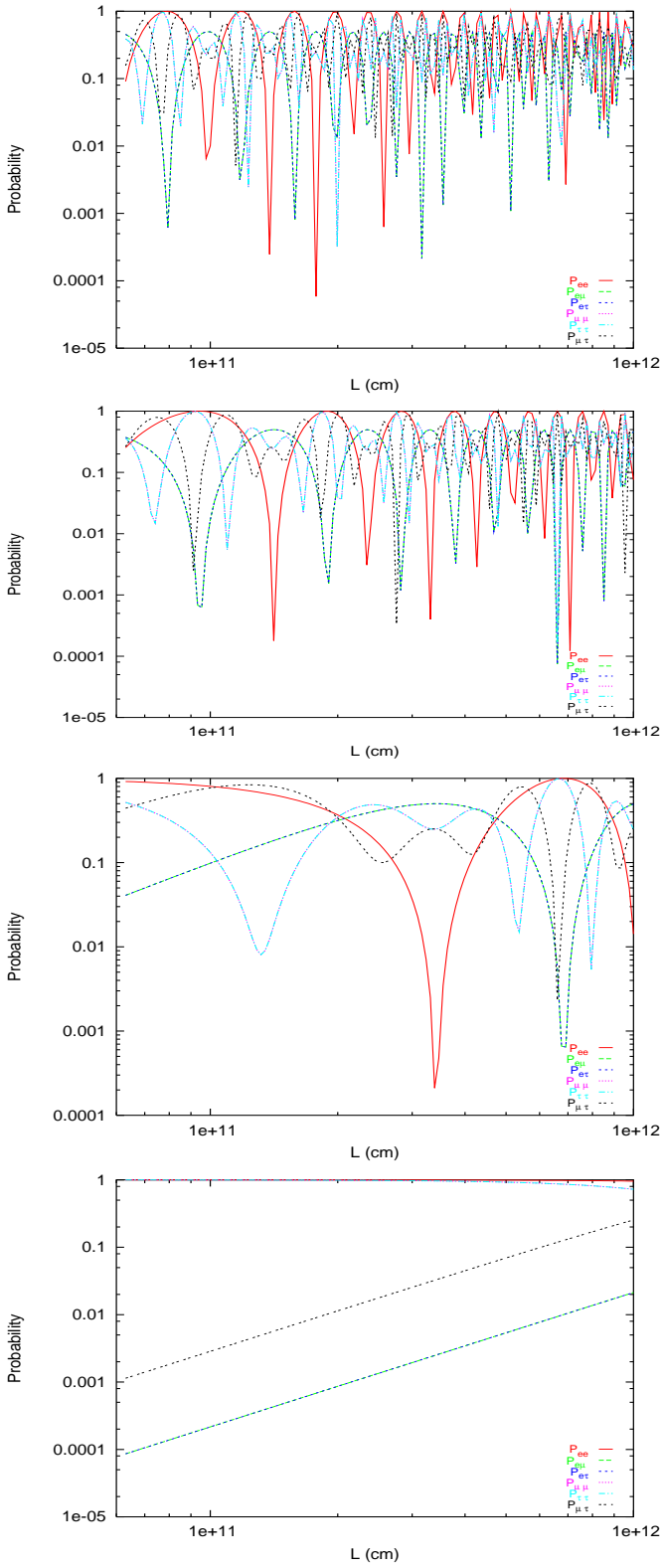


Figure 13. We plot the oscillation probability when neutrinos are produced at a radius $r = 6 \times 10^{10}$ cm and are propagating through the jet direction for four energies: $E_\nu = 178$ GeV (first figure), $E_\nu = 428$ GeV (second figure), $E_\nu = 3$ TeV (third figure) and $E_\nu = 69$ TeV (four figure)